University of Strathclyde

Lawrence Campbell,
James Henderson &
Brian McNeil,

Improving temporal coherence and generating shorter pulses in the FEL

David Dunning
& Neil Thompson

ASTeC

Outline

- Harmonic Lasing
- RAFEL
- Mode-locking amplifiers & oscillators for short pulse generation
- EEHG – another look at what can be done
- High Brightness SASE
- Puffin: A three dimensional, unaveraged free electron laser simulation code
- CLARA – a new UK test facility?

Harmonic Lasing

Harmonic Amplifier FEL*

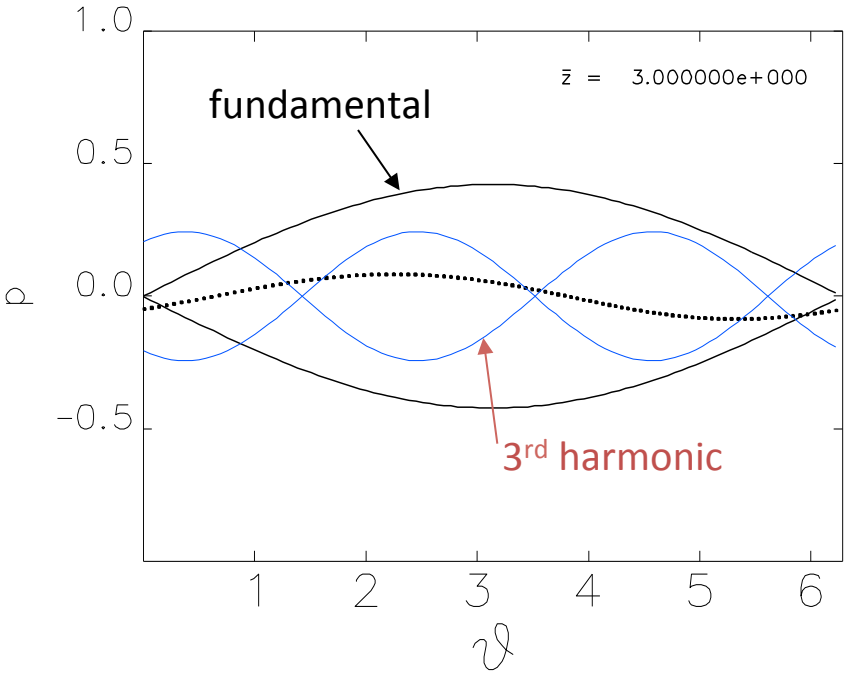

A relative phase change between electrons and fundamental radiation of $n2\pi/3$ (n - integer) will disrupt the fundamental-electron coupling and so the fundamental's growth.

However, A $n2\pi/3$ phase change for the fundamental is a $n2\pi$ phase change for the 3rd harmonic – The 3rd harmonic interaction therefore suffers no disruption.

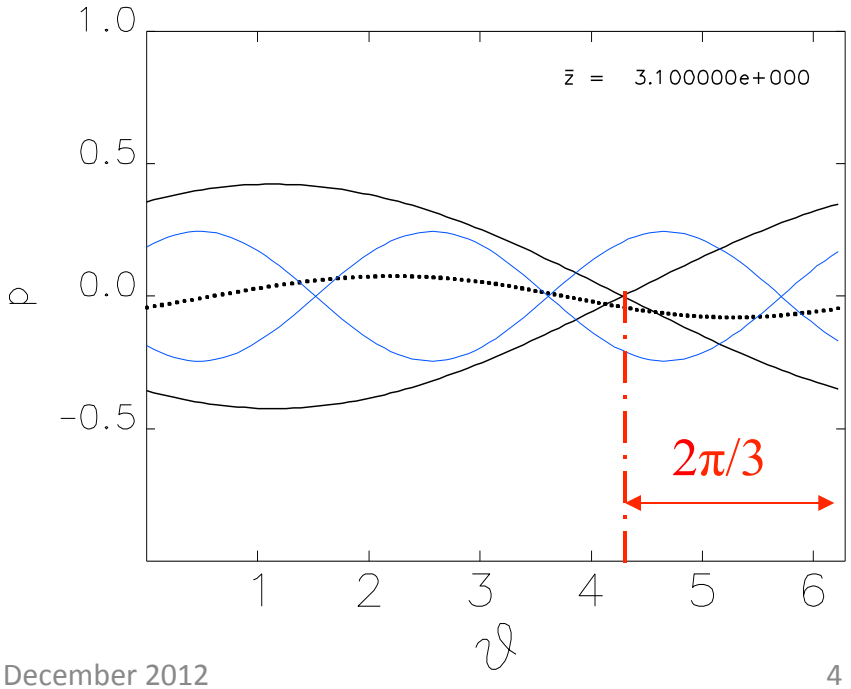

*McNeil, Robb & Poole, PAC 2005, Knoxville, Tennessee, 1718-20

Using a seeded steady-state model* (i.e. no pulses effects):

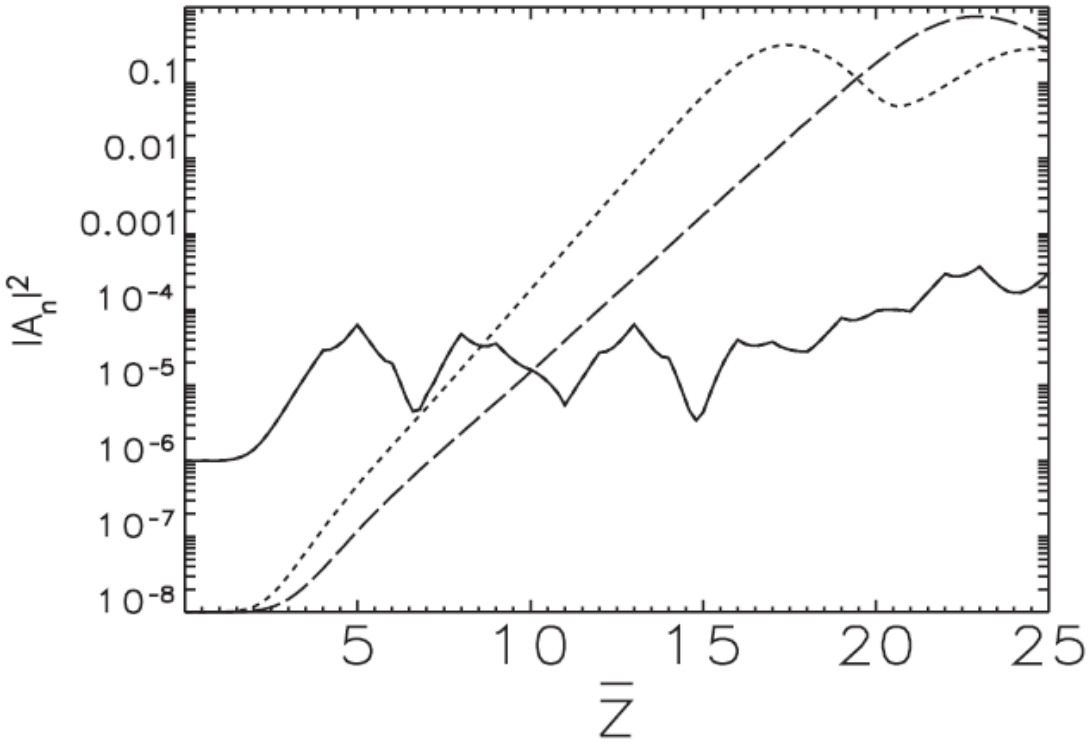

FIG. 2. Scaled powers of fundamental $|A_1|^2$ (solid line) and third harmonic $|A_3|^2$ (dotted line) for wiggler parameter $a_1 = 4$ demonstrating the effects of relative phase changes of $\Delta\theta = 2\pi/3$ at $\bar{z} = 4, 5, 6, \ldots, 24$. For the wiggler parameter retuned to $a_3 = 2.16$, A_3 is the fundamental and a separate simulation shows how $|A_3|^2$ (dashed line) evolves.

*McNeil, Robb, Poole & Thompson, PRL **96**, 084801 (2006)

Harmonic amplifier SASE optimisation simulations at LCLS and XFEL*

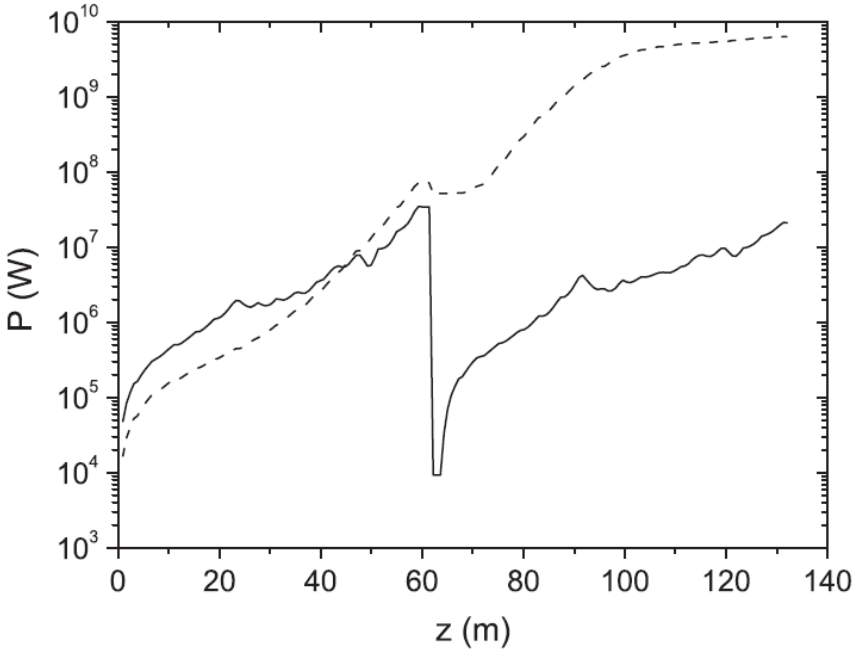

FIG. 7. Averaged peak power for the fundamental harmonic (solid) and the third harmonic (dash) versus geometrical length of the LCLS undulator (including breaks). The wavelength of the third harmonic is 0.5 Å (photon energy 25 keV). Beam and undulator parameters are in the text. The fundamental is disrupted with the help of the spectral filter (see the text) and of the phase shifters. The phase shifts are $4\pi/3$ after segments 1–5 and 17–22, and $2\pi/3$ after segments 6–10 and 23–28. Simulations were performed with the code FAST.

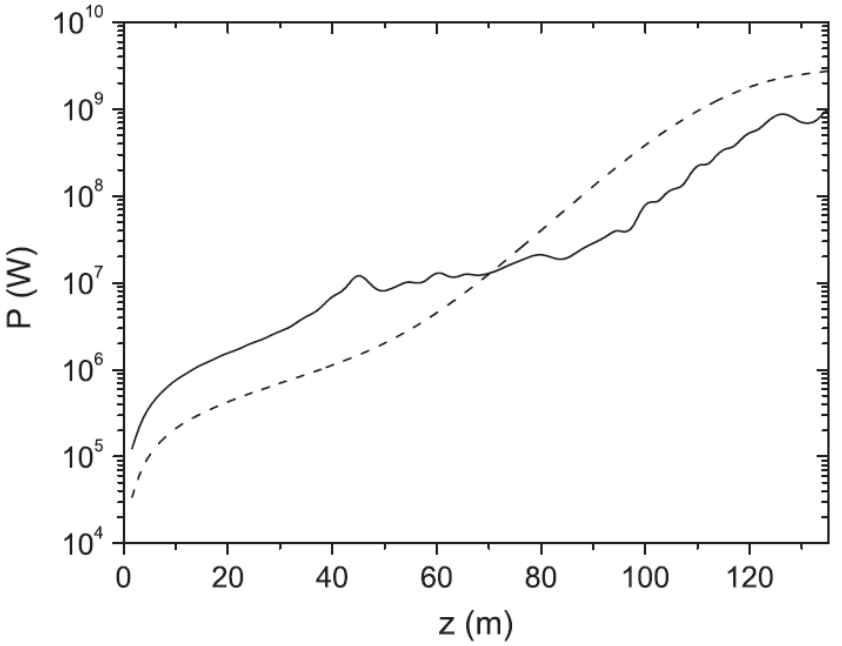

FIG. 8. An example for the European XFEL. Averaged peak power for the fundamental harmonic (solid) and the third harmonic (dash) versus magnetic length of SASE1 undulator. The wavelength of the third harmonic is 0.2 Å (photon energy 62 keV). The fundamental is disrupted with the help of phase shifters installed after 5 m long undulator segments. The phase shifts are $4\pi/3$ after segments 1–8 and 21–26, and $2\pi/3$ after segments 9–16. Simulations were performed with the code FAST.

*Schneidmiller & Yurkov, PRST-AB **15**, 080702 (2012)

Could be combined with a self-seeding method at fundamental.

Also works in FEL cavity oscillators for low gain*

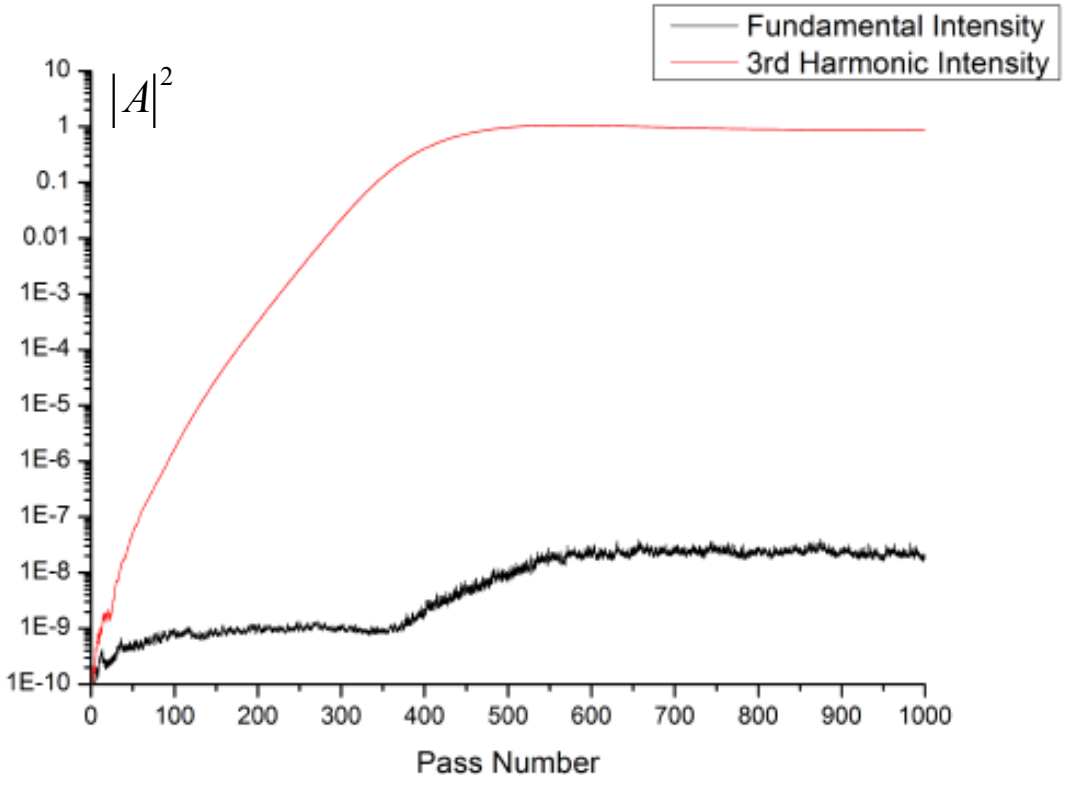

Such solutions are 'generic' and apply across all wavelength ranges from IR to X-ray (XFELO)

Parameter	Value
Electron pulse charge Q	80 pC
Pierce parameter ρ	$2.52 \times 10^{-}3$
Wiggler parameter a_w	4.0
Feedback factor F	0.99
Cavity detuning δ_c	0.00 l_c
No. of wiggler periods N_w	40
Wiggler length	1.27 l_g
No. of phase shifts $N_{\Delta\theta}$	19
Size of phase shifts $\Delta\theta$	$2\pi/3$

Table 5.2: Parameters used in the proof of concept test.

*Gavin Cheung (supervisor McNeil), *Modelling 4th Generation Light Sources*, Undergraduate Project Report, University of Strathclyde (April 2012).

...and in FEL cavity oscillators in the high gain (RAFEL)*

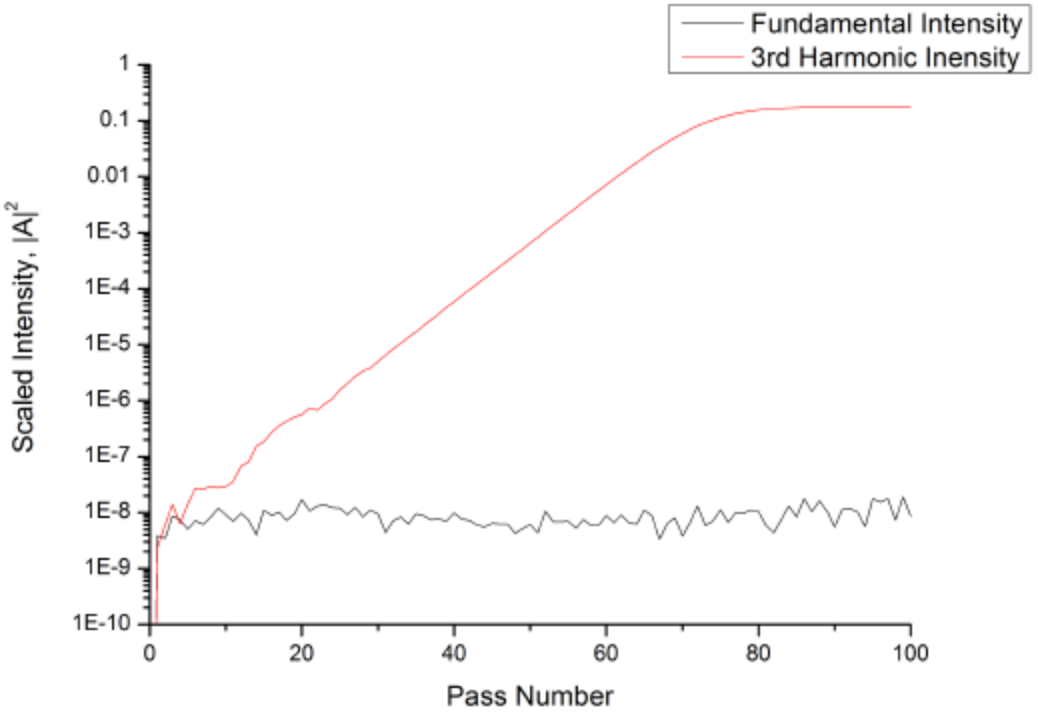

Such solutions are 'generic' and apply across all wavelength ranges from IR to X-ray (XFELO)

Parameter	Value
Electron pulse charge Q	200 pC
Pierce parameter ρ	2×10^{-3}
Wiggler parameter a_w	2.0
Feedback factor F	0.3
Cavity detuning δ_c	1 l_c
No. of wiggler periods N_w	290
No. of phase shifts $N_{\Delta\theta}$	57
Size of phase shifts $\Delta\theta$	$4\pi/3$

*Gavin Cheung (supervisor McNeil), *Modelling 4th Generation Light Sources*, Undergraduate Project Report, University of Strathclyde (April 2012).

RAFEL

Regenerative Amplifier FEL

- High Gain Low Feedback concept (Low-Q cavity)
  McNeil B W J 1990 *IEEE J. Quantum Electron.* **26** 1124

- Los Alamos IR-RAFEL
  Nguyen D C, Sheffield R L, Fortgang C M, Goldstein J C, Kinross-Wright J M and Ebrahim N A 1999 *Nucl. Instrum. Methods Phys. Res.* A **429** 125–30

- TTF VUV-RAFEL
  Faatz B, Feldhaus J, Krzywinski J, Saldin E L, Schneidmiller E A and Yurkov M V 1999 *Nucl. Instrum. Methods Phys. Res.* A **429** 424–8

- LCLS X-RAY RAFEL
  Huang Z and Ruth R D 2006 *Phys. Rev. Lett.* **96** 144801

As well as these experiments in the infrared region of the spectrum, this high-gain regime of the FEL oscillator is also of interest in FEL designs for the ultraviolet and higher frequencies. The lack of high mirror reflectivities for these frequencies severely restricts the design of low-gain oscillators.

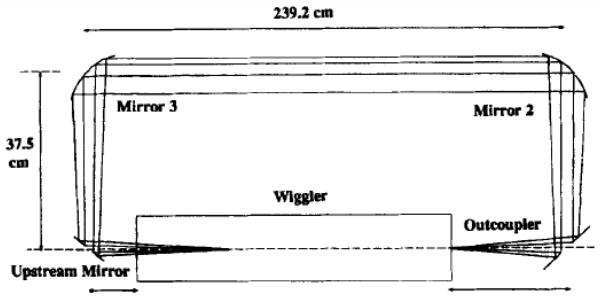

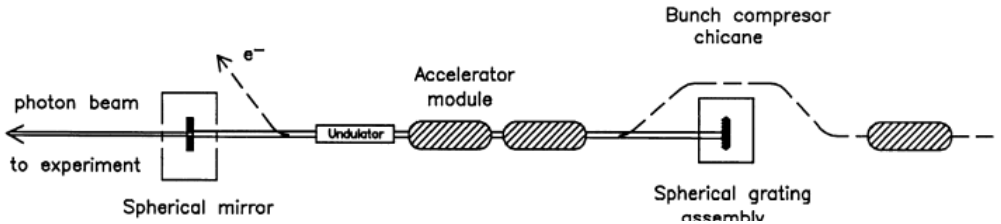

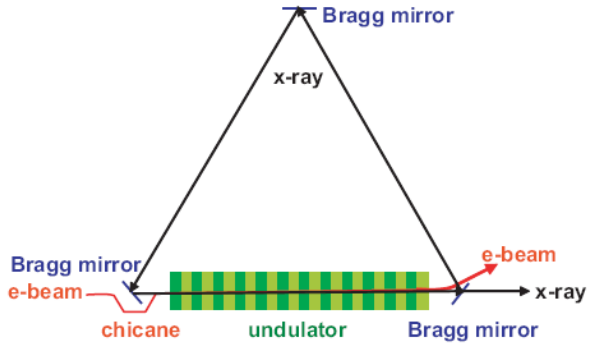

UK RAFEL in 4GLS*

Table 1. Predicted VUV-FEL radiation output.

Tuning range	~3–10 eV
Peak power	~500–300 MW (3 GW[a])
Repetition rate	$n \times 4\frac{1}{3}$ MHz ($n \leqslant 300$, integer)
Polarization	Variable elliptical
Min pulse duration FWHM	170 fs (25 fs[a])
Typical $\Delta\nu\Delta t$	~1.0
Maximum pulse energy	70 μJ
Maximum average power	$n \times 300$ W

[a]Indicates possible output in superradiant mode of operation.

*Thompson, Poole & McNeil, Proc. FEL 2005, Stanford, **MOPP024**, 79-82 (2005)

*McNeil, Thompson, Dunning, Karssenberg, van der Slot & Boller, New Journal of Physics **9** 239 (2007)

WHY A RAFEL?*

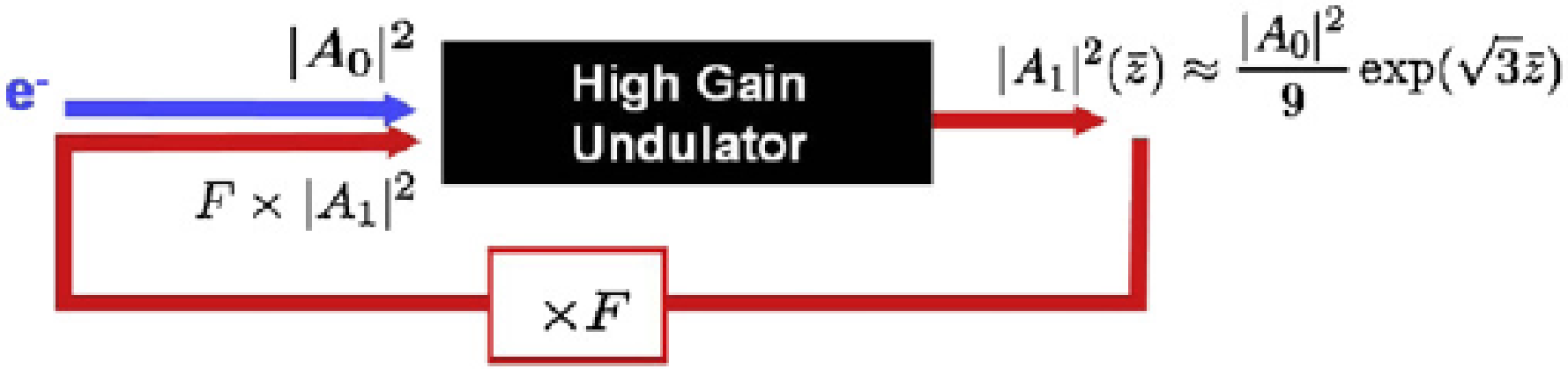

Fig. 1. Schematic representation of a generic high gain RAFEL system.

- Robust FEL cavity design able to generate close to Fourier Transform limited tuneable output from feedback factors F 10^{-5} : a self-seeding high gain FEL **ideal for short wavelength generation**

*Dunning, McNeil & Thompson, NIM A **593**, 116-9 (2008)

Example short-pulse RAFEL simulation*

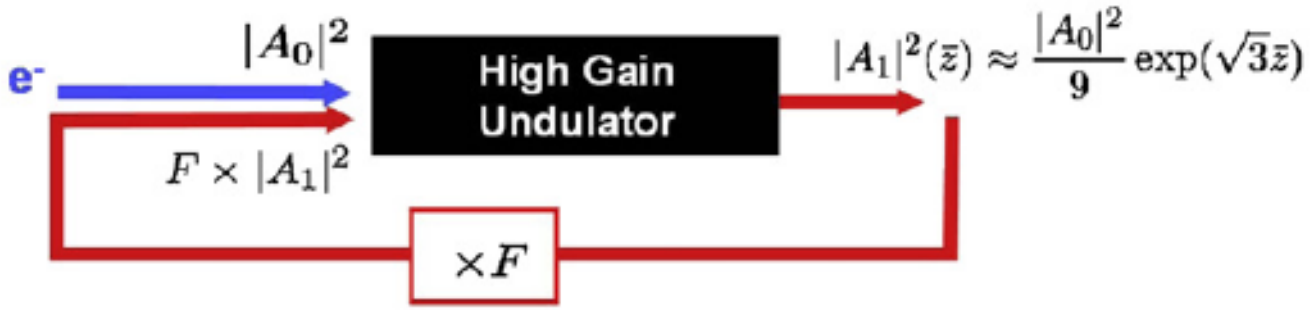

Fig. 1. Schematic representation of a generic high gain RAFEL system.

Parameters are typical for a soft x-ray FEL:

Gaussian current electron pulse:	$\sigma_z = l_c \quad \left(l_c = \lambda/4\pi\rho\right)$
FEL parameter:	$\rho = 2\times10^{-3}$
Undulator length:	$L_u = 6\,l_g \quad \left(l_g = \lambda_u/4\pi\rho\right)$
Cavity feedback factor:	$F = 4\times10^{-3}$
Cavity detuning:	shortened by $2l_c$

*McNeil & Thompson, EPL, **96**, 5400 (2011) & **98**, 29901 (2012)

Short pulse RAFEL – stable, coherent output*

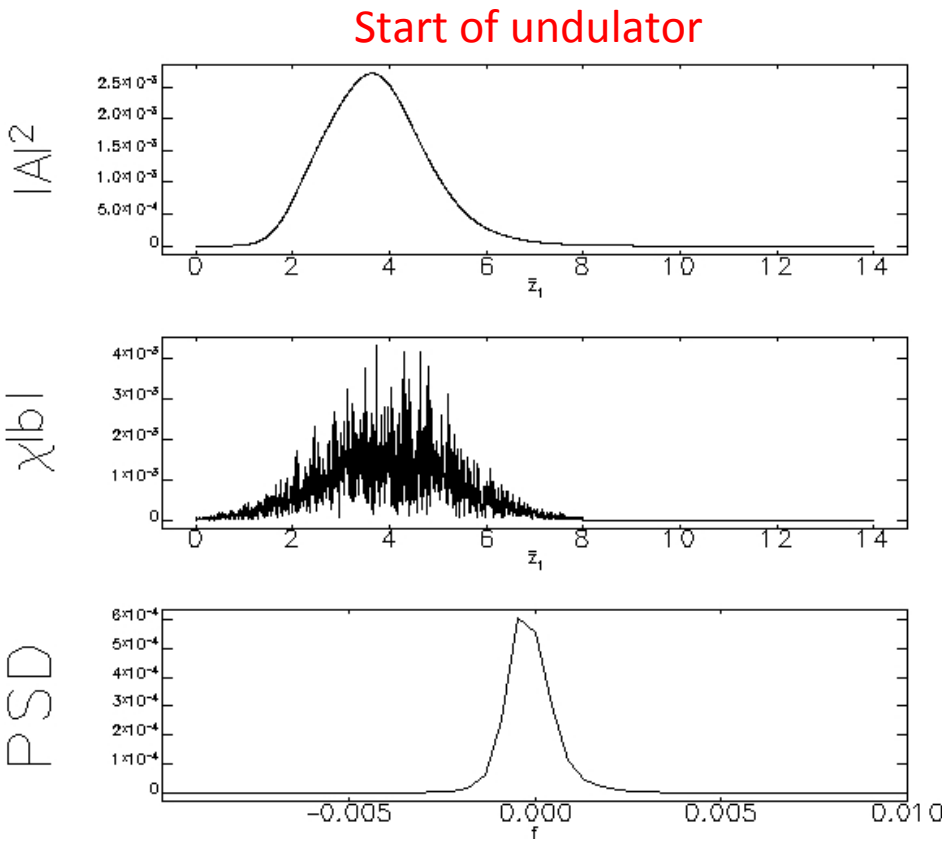

Figure 1: Short pulse RAFEL simulation - showing saturated evolution at the undulator entrance. From top: scaled power at the beginning of the interaction at saturation; the current-weighted bunching; the scaled spectral power as a function of scaled frequency.

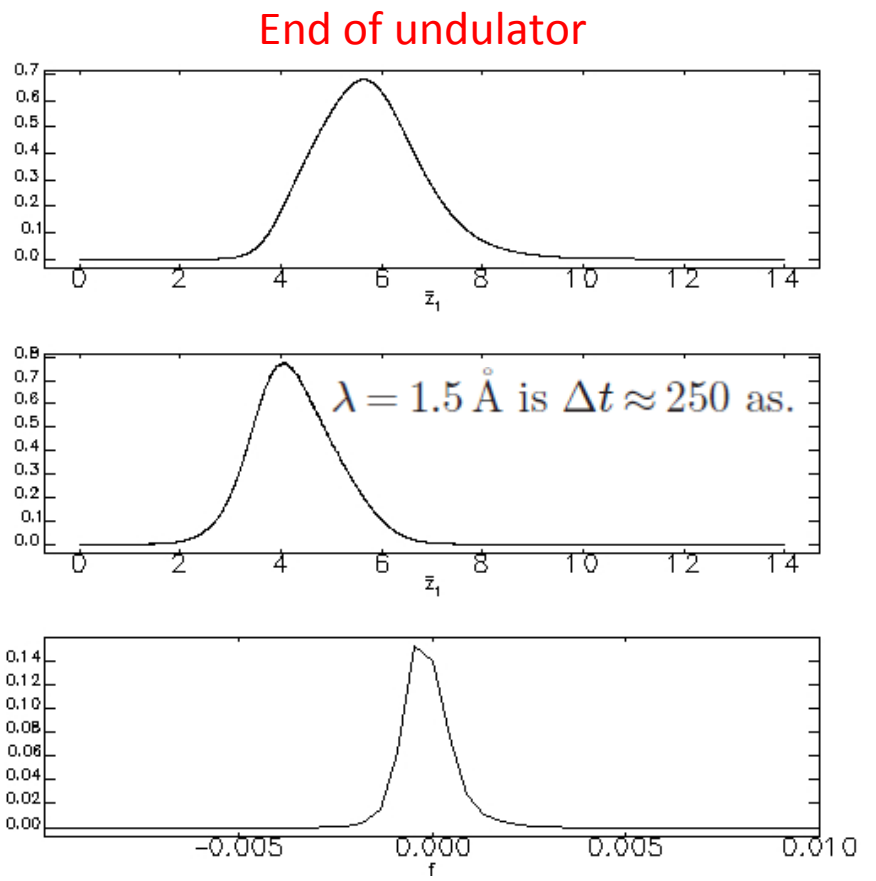

Figure 2: Short pulse RAFEL simulation - showing saturated evolution at the undulator exit.

Short (: l_d), high power, FT limited pulses with none of the jitter associated with SASE.

*McNeil & Thompson, EPL, **96**, 5400 (2011) & **98**, 29901 (2012)

Mode-locking amplifiers & oscillators for short pulse generation

Axial Modes from an *amplifier* FEL

- ***Synthesise axial mode spectrum without cavity***

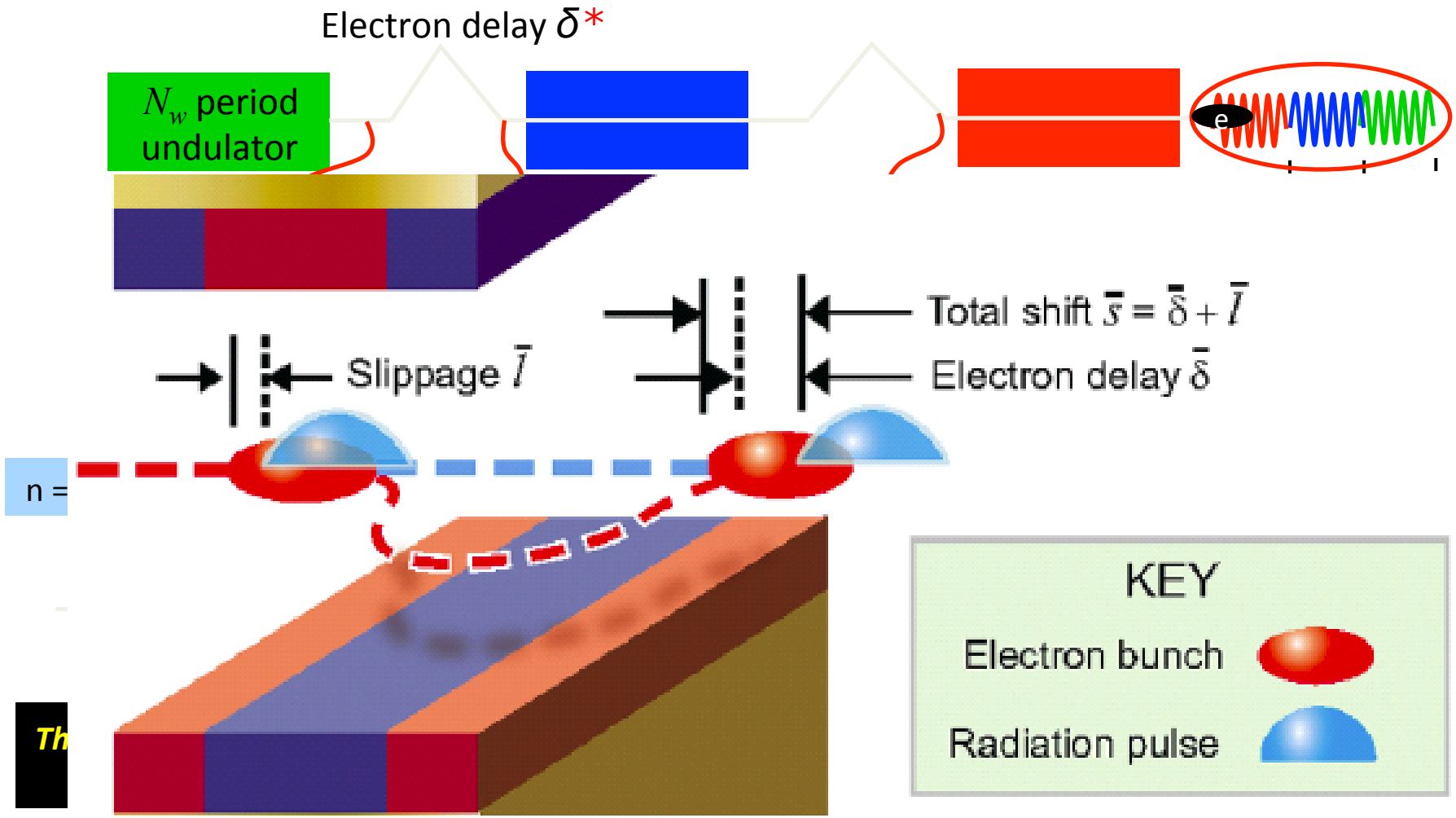

*Jones, Clarke & Thompson, IPAC 2012, USA, 1759 (2012). (For 'dispersionless' chicanes)

Mode generation

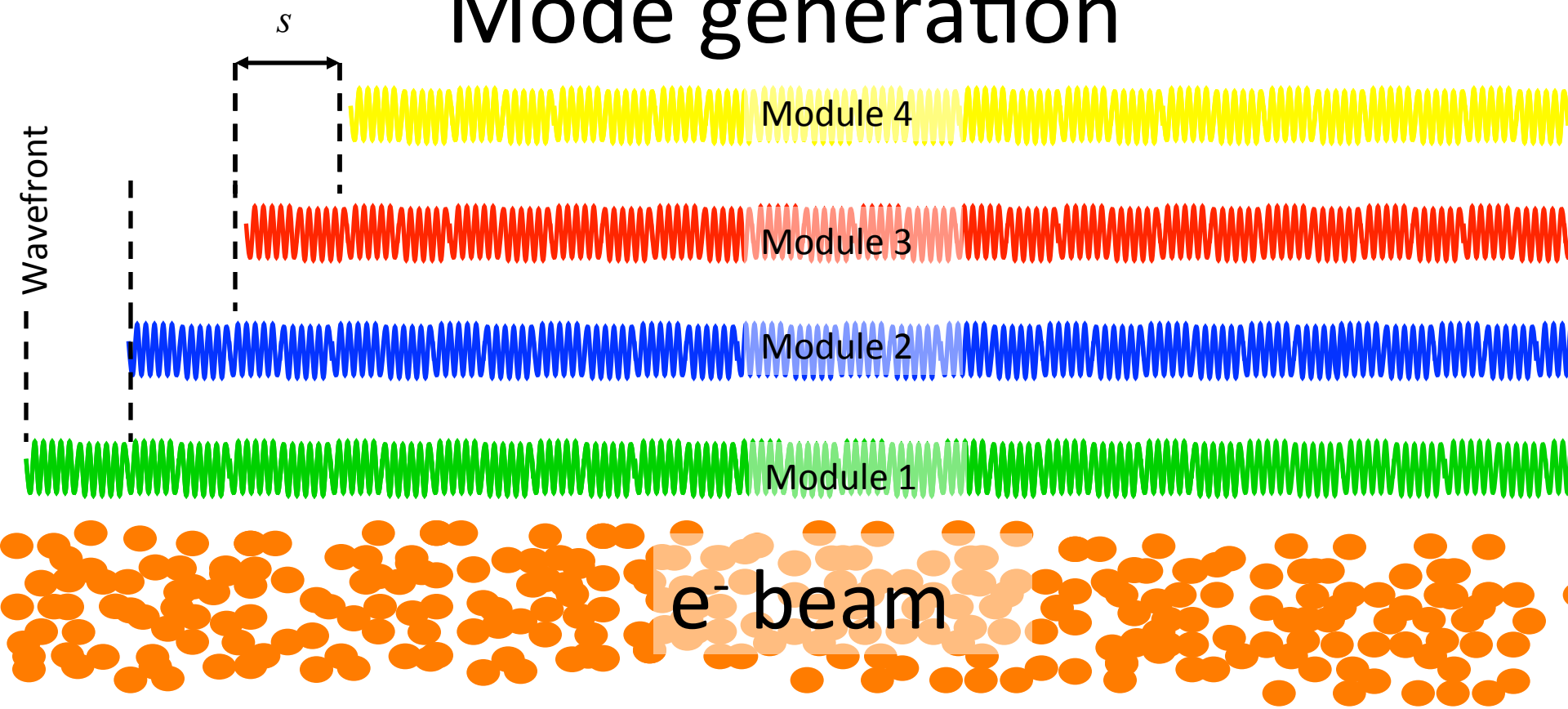

For continued slips of distance s, only those wavelengths with an integer number of periods in distance s will survive after many such slips. For s an integer of λ_j:

$$s = N\lambda_j = (N+1)\lambda_{j-1}$$

$$\Rightarrow \omega_j = \frac{2\pi cN}{s};\ \omega_{j-1} = \frac{2\pi c(N+1)}{s} \quad \Rightarrow \Delta\omega_s = \omega_{j-1} - \omega_j = \frac{2\pi c}{s}$$

X-ray SASE MLOK amplifier with mode-locking*

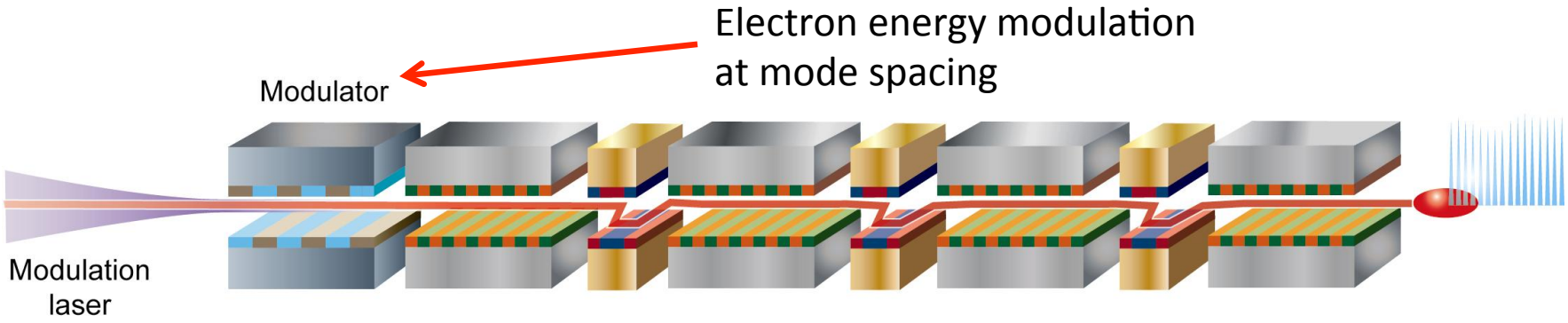

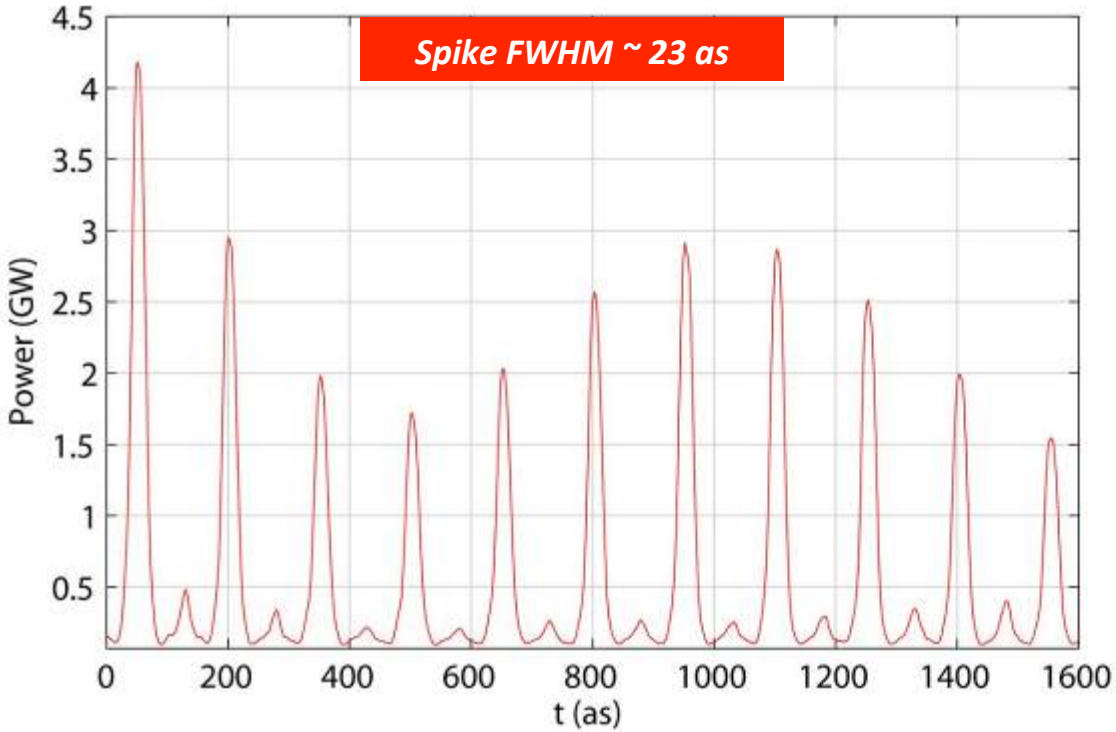

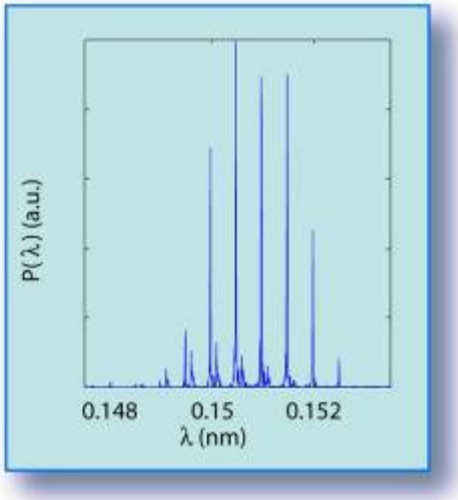

*Thompson, McNeil, PRL **100,** 203901 (2008)

MLOK with current modulation*

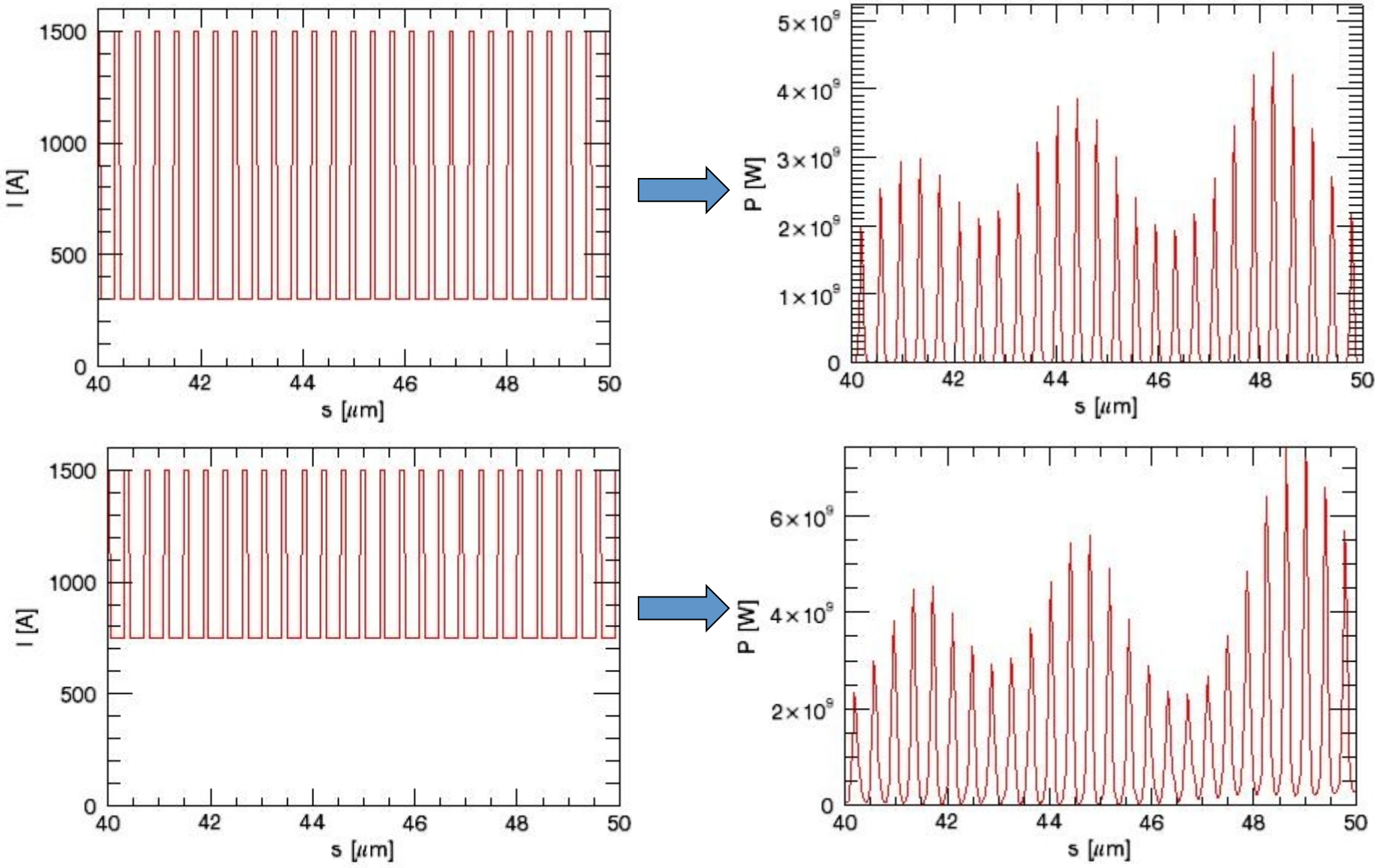

*Kur, Dunning, McNeil, Wurtele & Zholents, New Journal of Physics **13**, 063012 (2011)

Amplified HHG – retaining structure with MLOK*

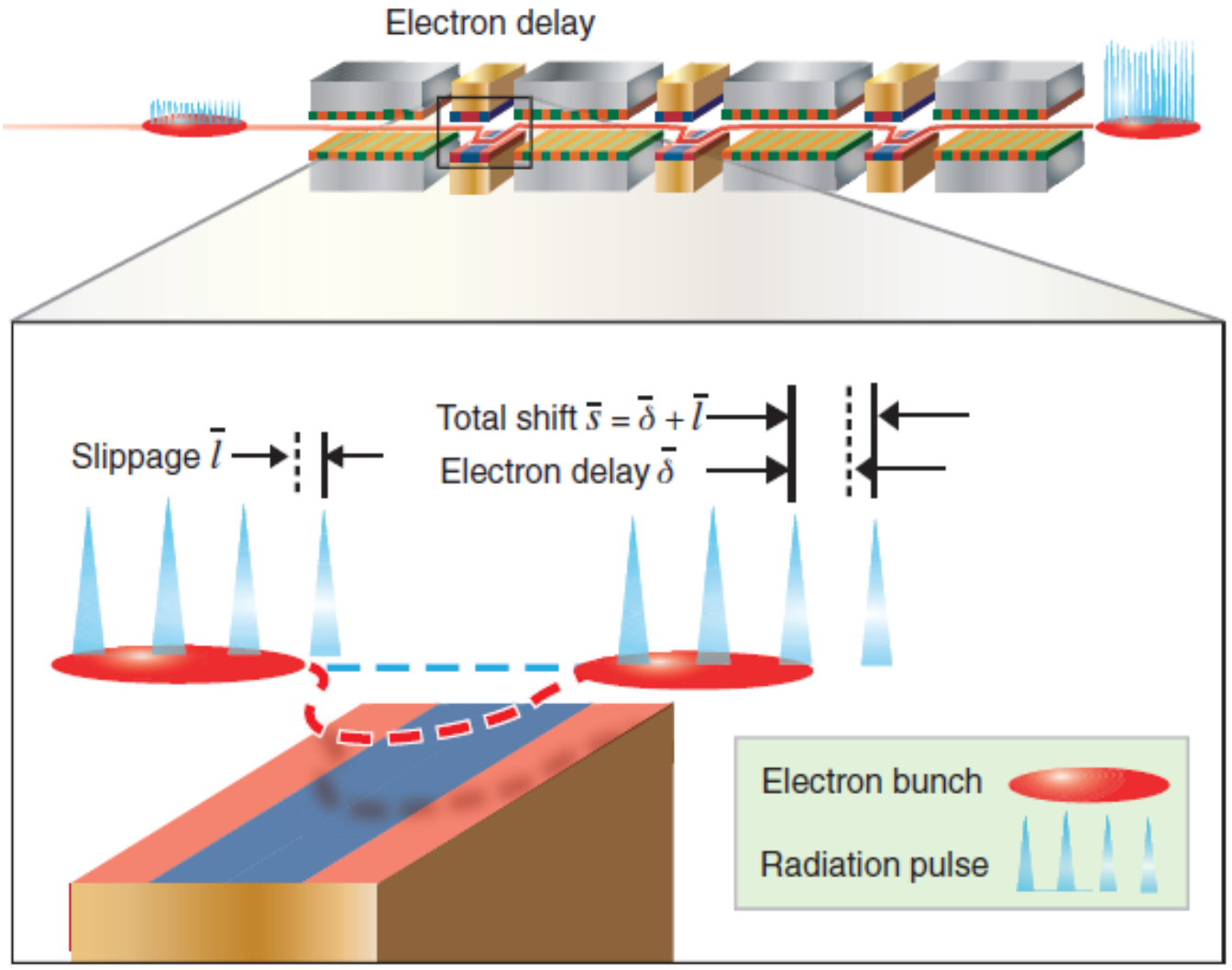

*McNeil, Thompson, Dunning, Sheehy, J. Phys. B: At. Mol. Opt. Phys. **44**, 065404 (2011)

Amplified HHG – retaining structure with MLOK

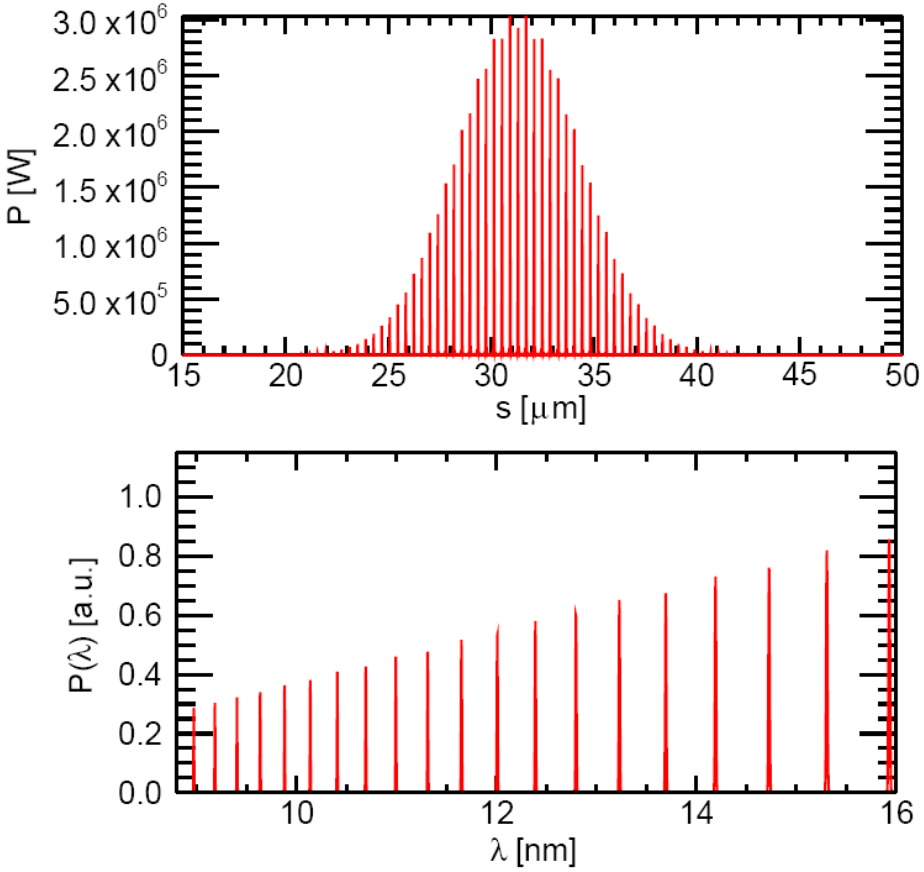

Fig. 7: Longitudinal intensity profile (top) and spectral power distribution (bottom) of the HH seed in 3D simulations.

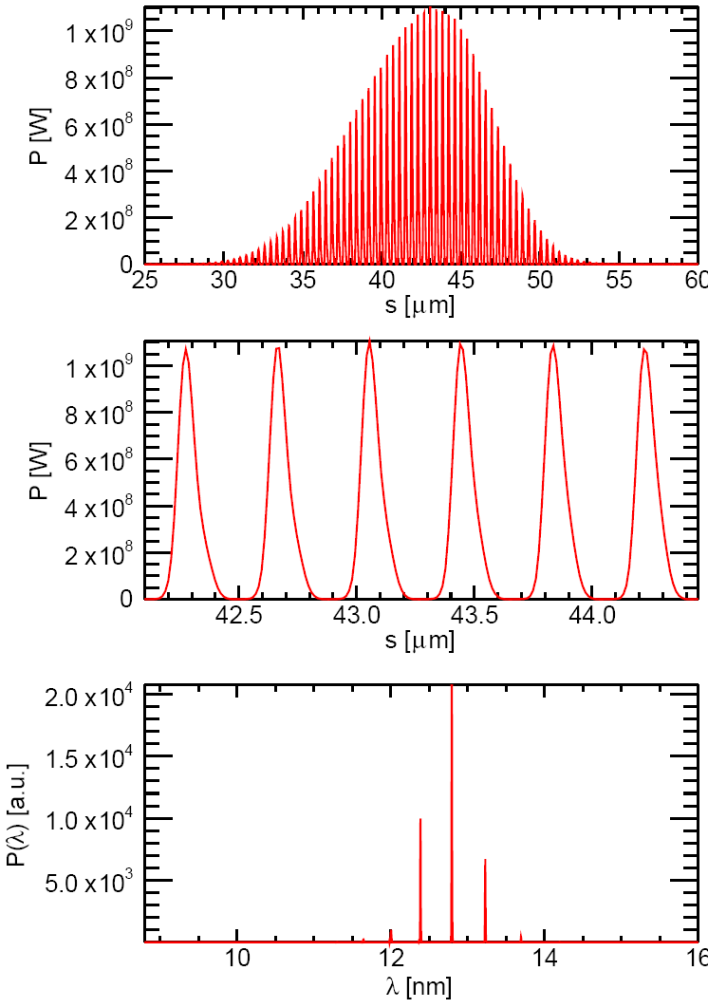

Fig. 8: Longitudinal intensity profile (top and middle) ar spectral power distribution (bottom) of the amplified HH r diation in 3D simulations, with $S_e = 8$. The agreement wit the equivalent 1D simulations shown in Fig. 6 is very good.

3D Genesis simulations for $\lambda_r \approx 12$ nm

Start-to-end simulations*

Input for NLS – like parameters

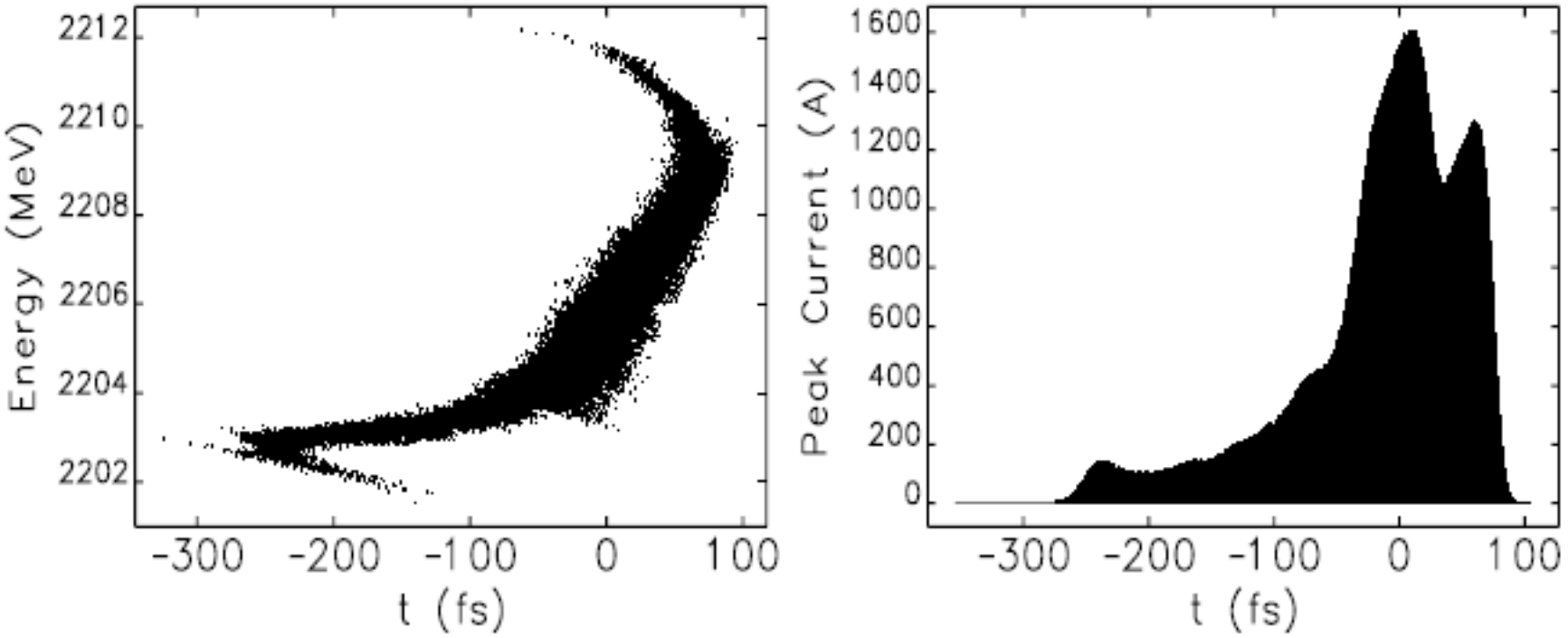

*Dunning, McNeil, Thompson, Williams, Phys. Plasmas **18**, 073104 (2011)

Start-to-end simulations - output

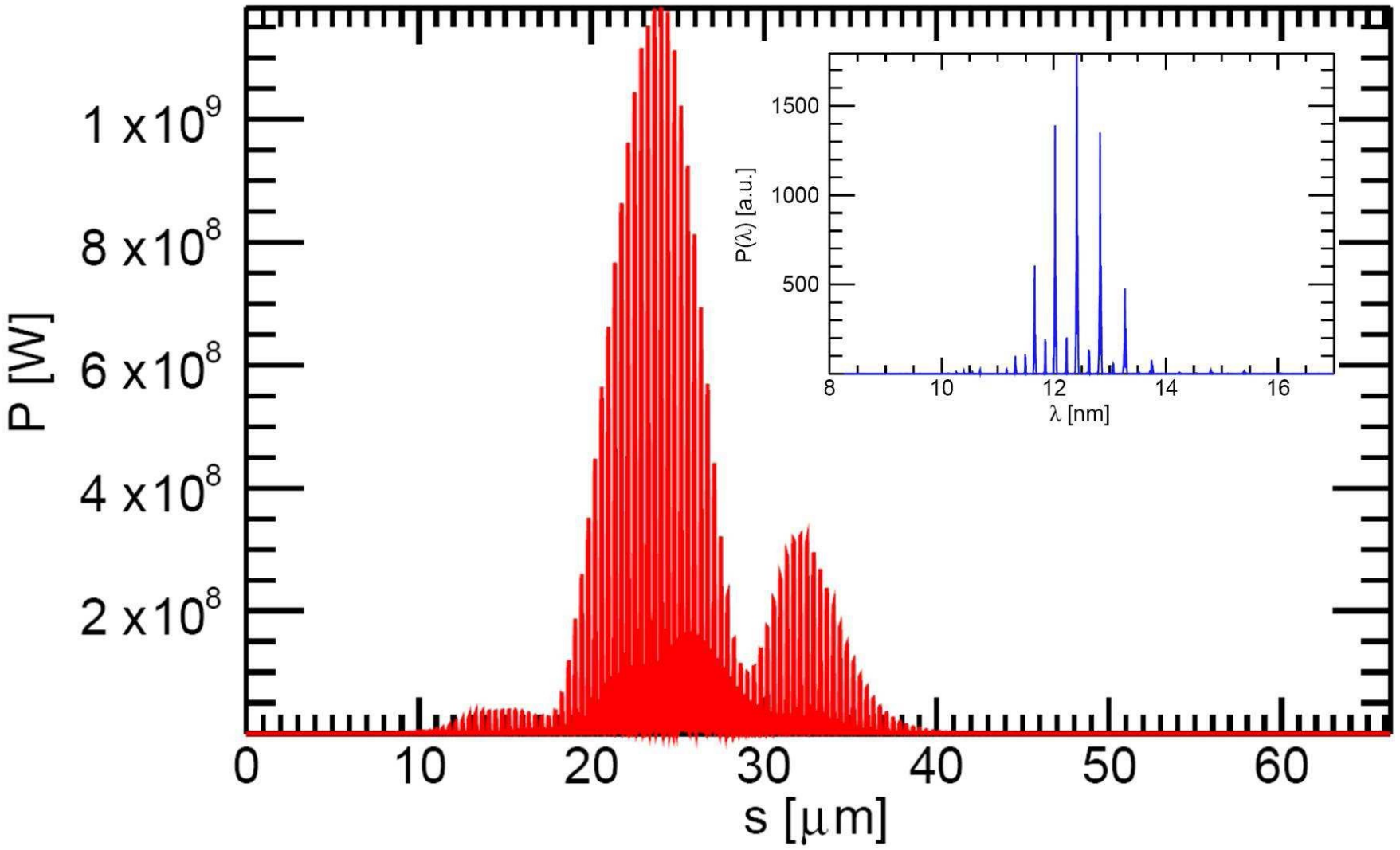

RAFEL in MLOK configuration*

Start of undulator

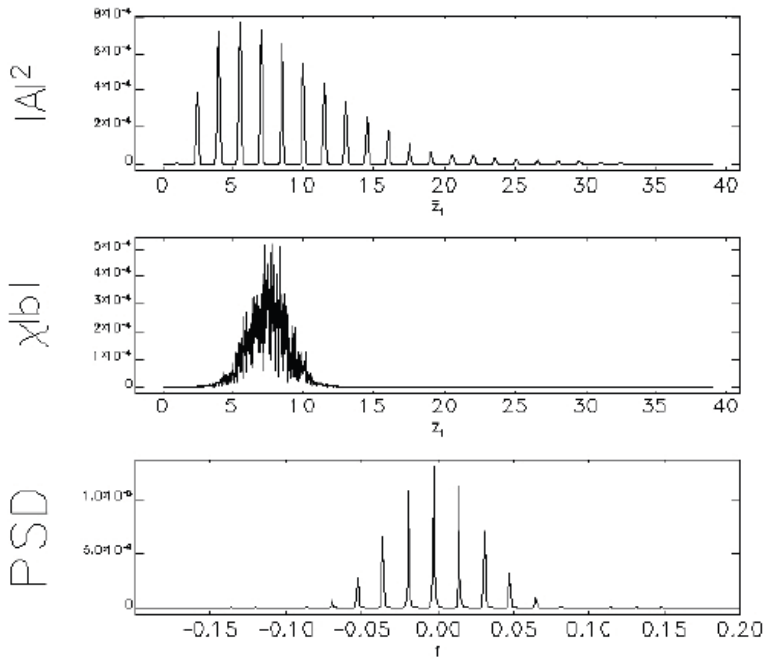

Fig. 3: Short-pulse MLOK RAFEL simulation —showing saturated evolution at the undulator entrance. From top: scaled power at the beginning of the interaction at saturation; the current-weighted bunching; the scaled spectral power as a function of scaled frequency.

End of undulator

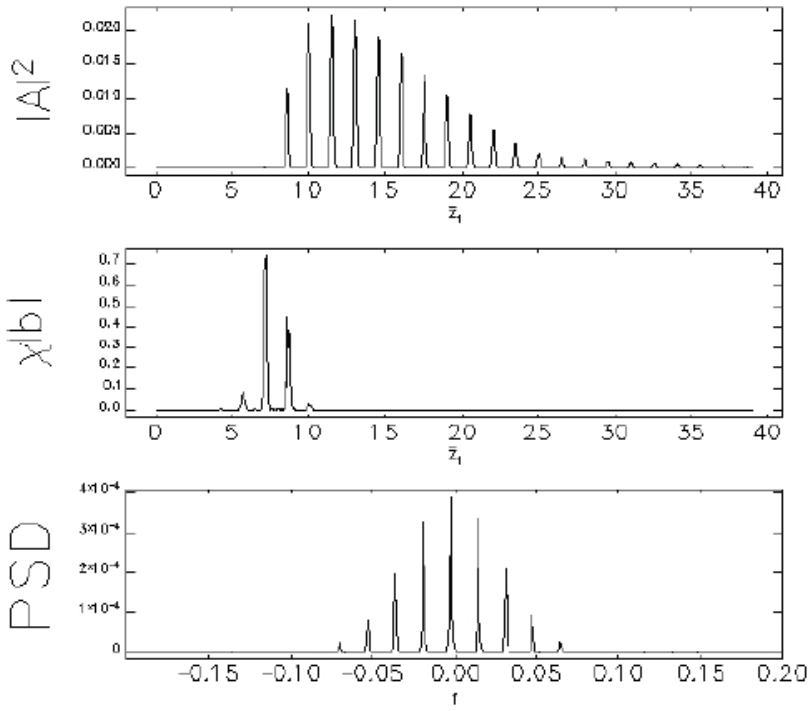

Fig. 4: Short-pulse MLOK RAFEL simulation —showing saturated evolution at the undulator exit.

*McNeil & Thompson, EPL, **96**, 5400 (2011) &
98, 29901 (2012)

Mode Locked After Burner*

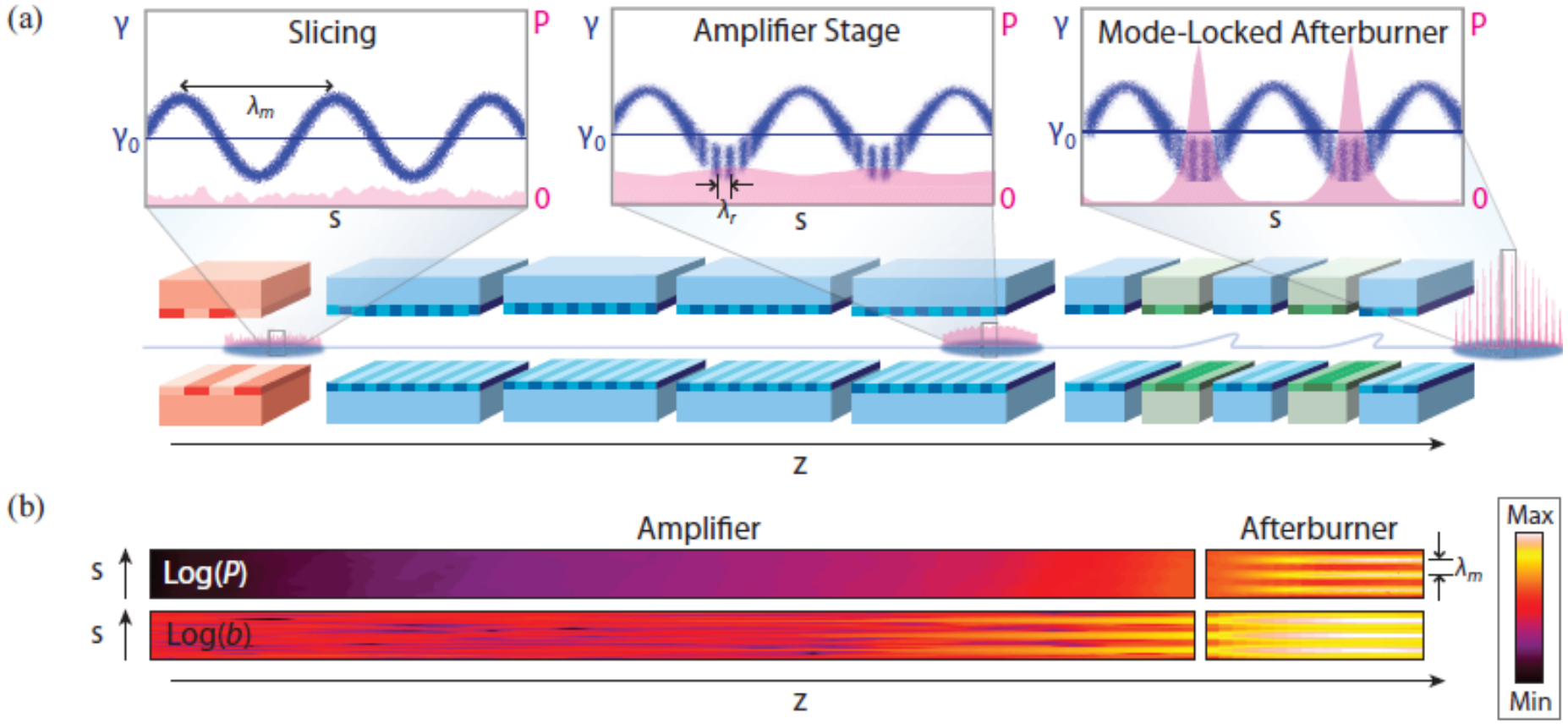

*Dunning, McNeil & Thompson, '*Few Cycle Pulse Generation in and X-ray Free Electron Laser*', http://arxiv.org/pdf/1212.2047v1.pdf

TABLE I: Parameters for soft and hard x-ray simulations.

Parameter	Soft x-ray	Hard x-ray
Amplifier stage		
Electron beam energy [GeV]	2.25	8.5
Peak current [kA]	1.1	2.6
ρ-parameter	1.6×10^{-3}	6×10^{-4}
Normalised emittance [mm-mrad]	0.3	0.3
RMS energy spread, σ_γ/γ_0	0.007 %	0.006 %
Undulator period, λ_u [cm]	3.2	1.8
Undulator periods per module	78	277
Resonant wavelength, λ_r [nm]	1.24	0.1
Modulation period, λ_m [nm]	38.44	3
Modulation amplitude, γ_m/γ_0	0.1 %	0.06 %
Extraction point [m]	34.1	36.0
Mode-locked afterburner		
Undulator periods per module	8	8
Chicane delays [nm]	28.52	2.2
No. of undulator-chicane modules	~15	~40

Optimum for:

$\gamma_m/\gamma_0 \approx \rho$

Soft X-ray Genesis simulation

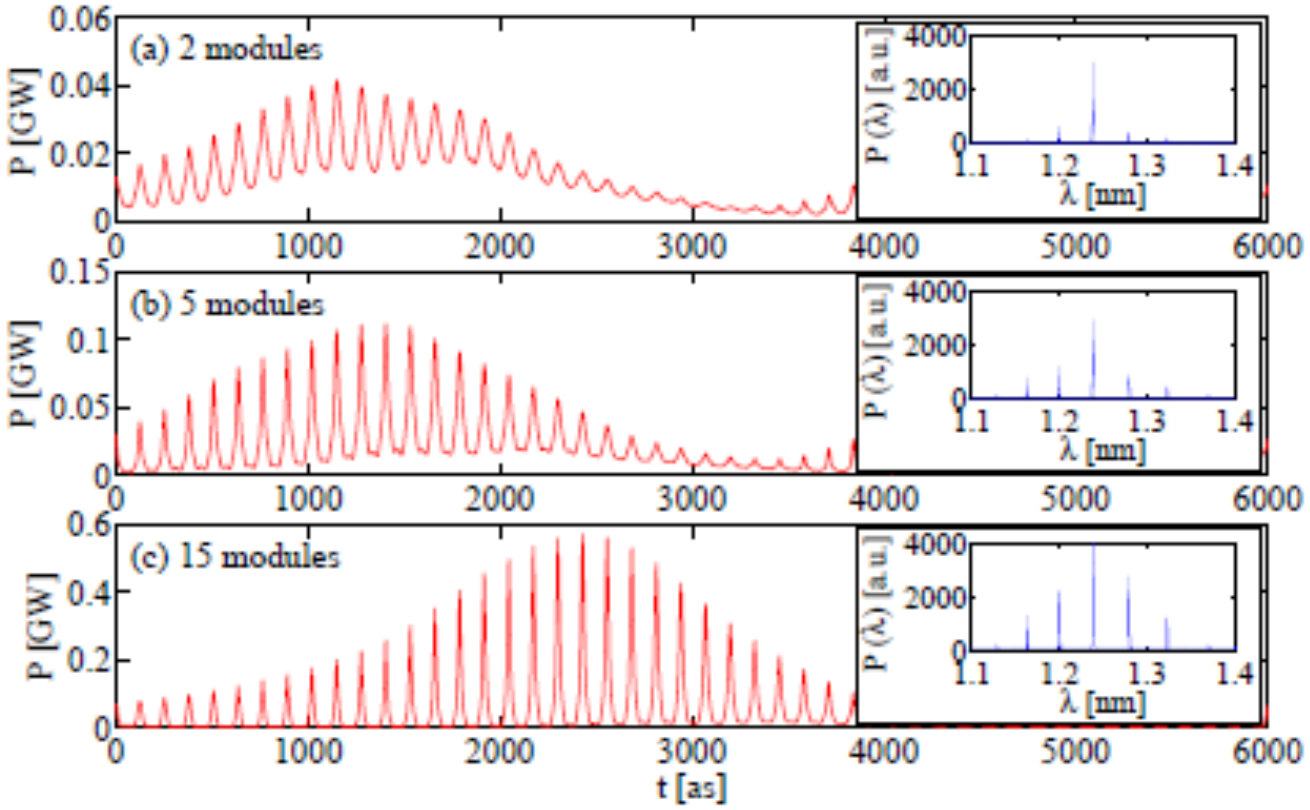

FIG. 3: Soft x-ray mode-locked afterburner simulation results: Radiation power profile and spectrum after (a) 2, (b) 5 and (c) 15 undulator-chicane modules. The duration of an individual pulse after 15 modules is ∼9 as rms.

Hard X-ray Genesis simulation

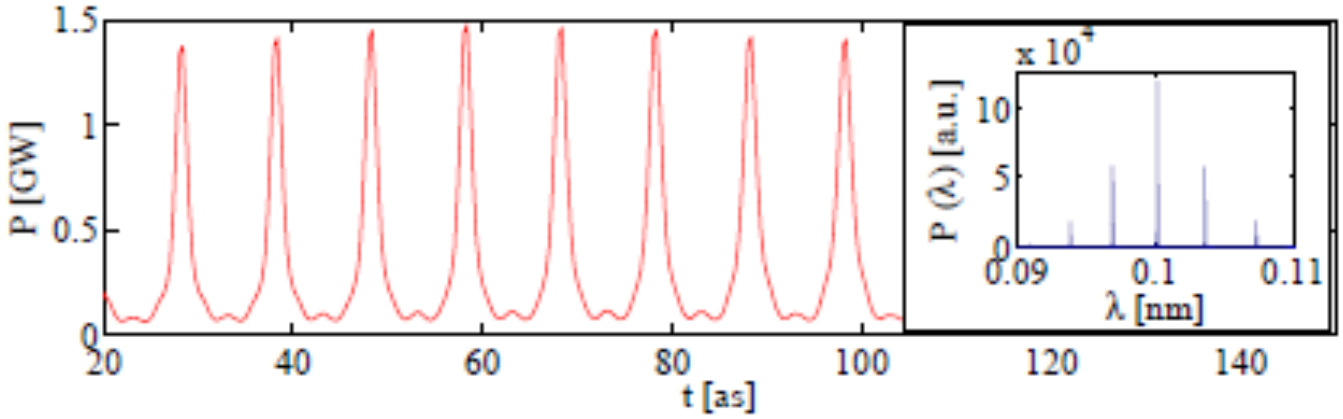

FIG. 4: Hard x-ray mode-locked afterburner simulation results: Radiation power profile and spectrum after 40 modules. The duration of an individual pulse is ~700 zs rms.

~5 optical cycles FWHM were attained

A (fantasy?) projection of these results to the LANL MaRIE proposal* for $\lambda_r \approx 0.25$ Å (50 keV photons) gives RMS pulse durations of 140 zs. These parameters allow us to consider experiments involving observation of electronic/nuclear and towards nuclear behaviour.

* B.E. Carlsten *et al.*, Proceedings of 2011 Particle Accelerator Conference, New York, NY, USA, **TUODS1**, 799-801 (2011).

EEHG – another look at what can be done

EEHG mechanism*

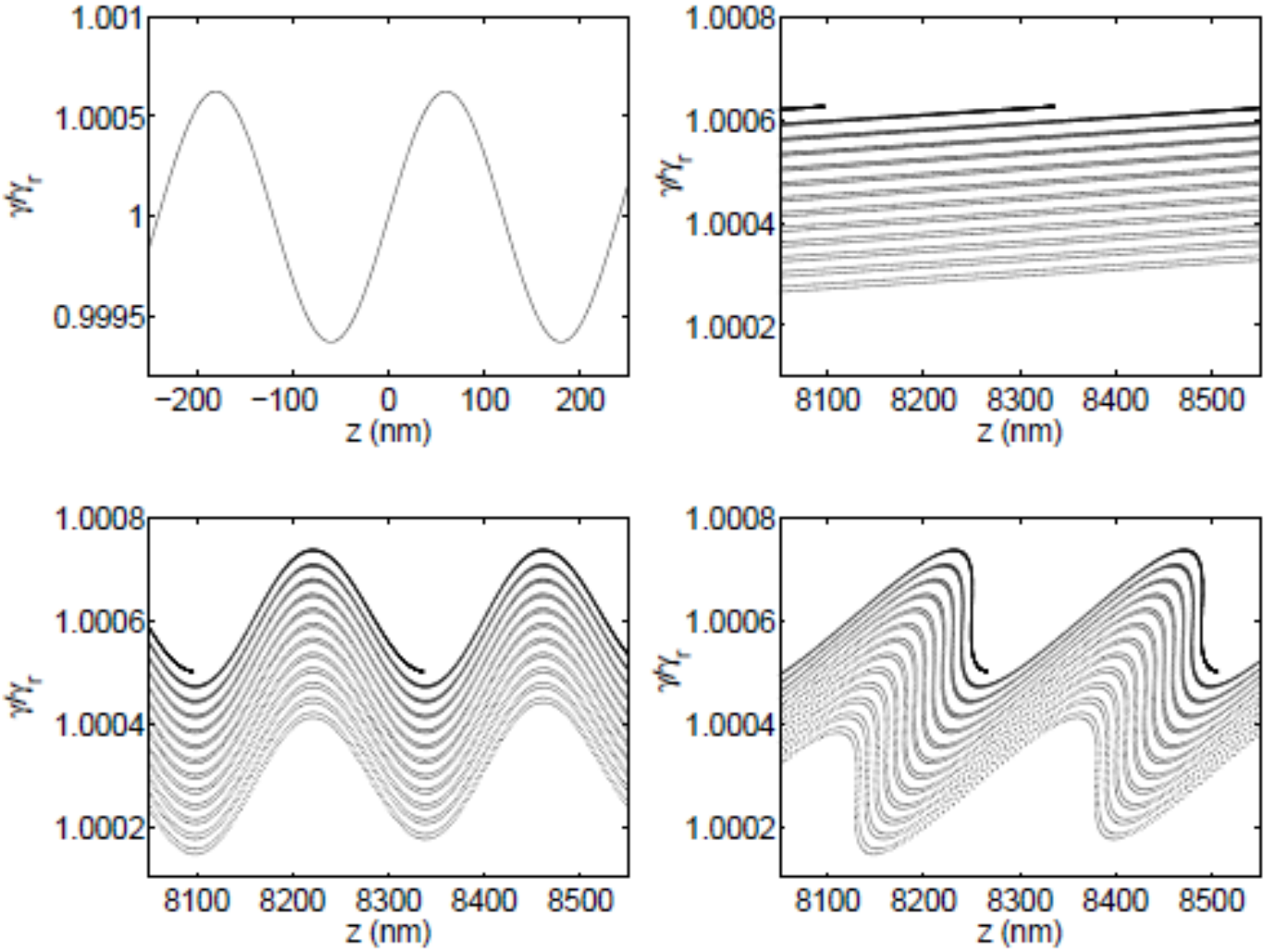

*Stupakov, Phys. Rev. Lett. **102**, 074801 (2009)

EEHG without periodic BC's or averaging*

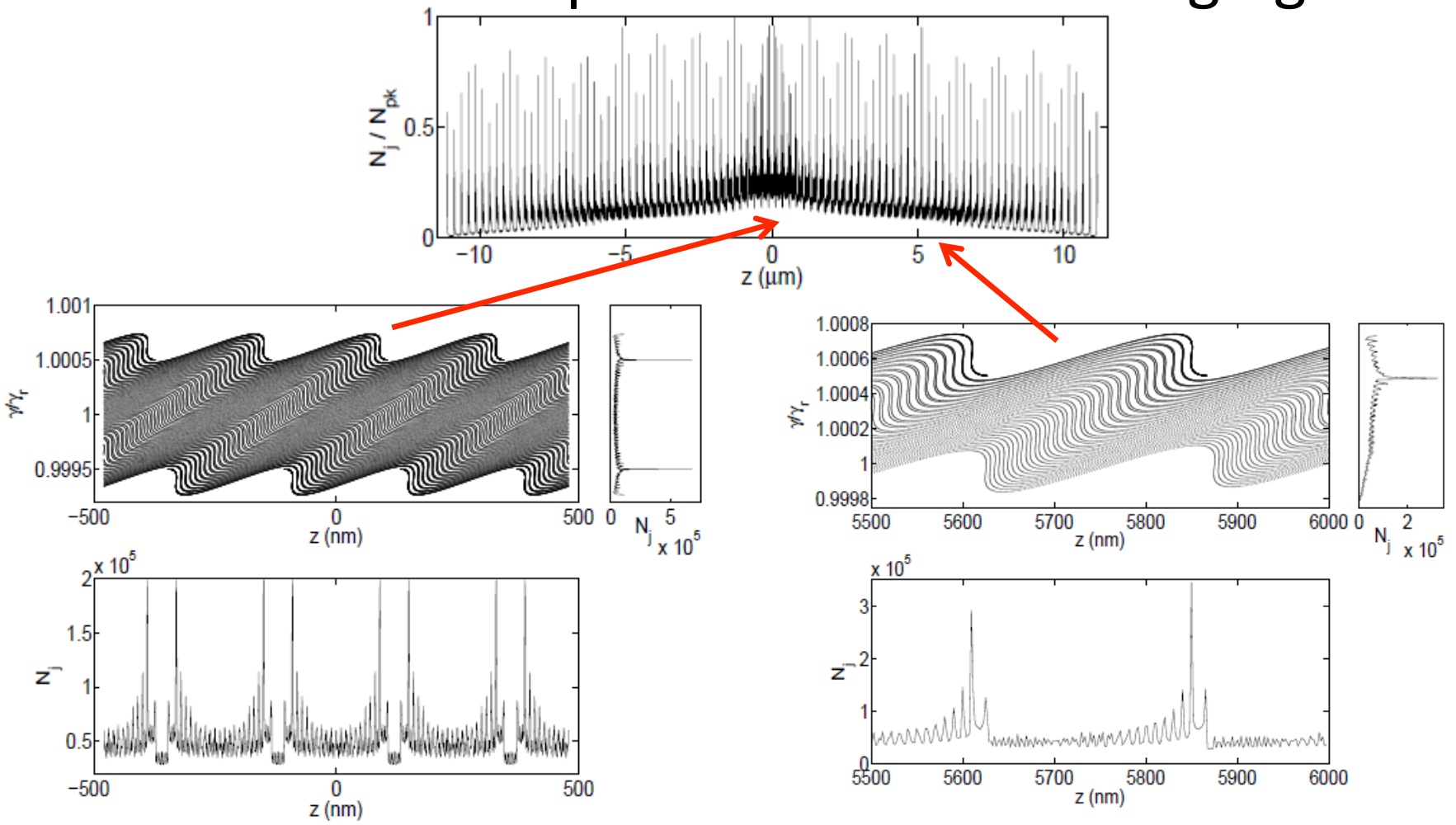

Fig. 1: Electron phase space (top) and histogram of electron numbers (bottom) about the centre of the electron pulse at $z = 0$. The particle density is increased for the higher energy electrons as is indicated by the top right plot.

Fig. 2: Electron phase space (top) and histogram of electron numbers (bottom) at the head of the electron pulse. The particle density is increased for the higher energy electrons as is indicated by the top right plot. Single current bands can be seen in the region around $z = 5600 - 5615$ nm with double current bands around $z = 5620 - 5830$ nm.

*Henderson, McNeil, *'Echo enabled harmonic generation free electron laser in a mode locked configuration'*, to be published in EPL

Normal radiator undulator

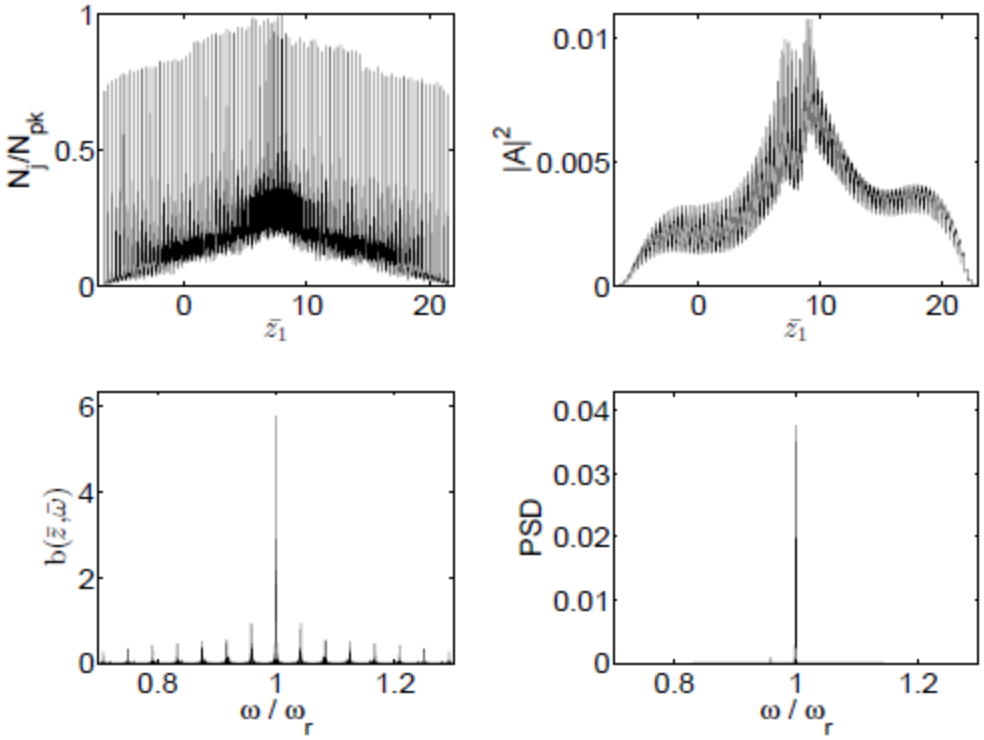

$\lambda_r \approx 10$ nm

Fig. 5: Electron and radiation pulse at saturation in a simple undulator at $\bar{z} \approx 1.1$ for the normal EEHG case. Plots on the left are: top - normalised electron number histogram (bin size $= \lambda_r/5$); bottom - Fourier transform of bunching $b(\bar{z}, \bar{\omega})$. On the right: top - radiation field amplitude $|A|^2$ as a function of $\bar{z}_1$; bottom - scaled Power Spectral Density showing emission at resonance dominates.

MLOK radiator undulator

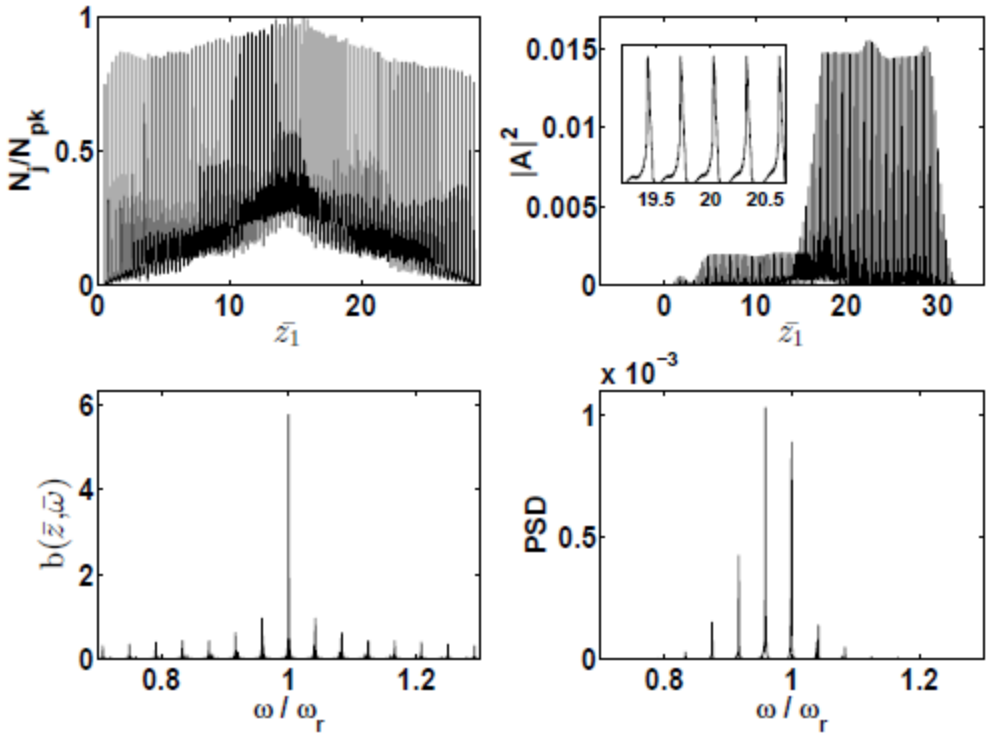

$\lambda_r \approx 10$ nm

The visibility of radiation pulse train structure is defined as $V = (|A|^2_{max} - |A|^2_{min})/(|A|^2_{max} + |A|^2_{min})$, were the maximum and minimum values are defined between two adjacent peaks. The effect of introducing an energy spread σ_E in the initial electron pulse energy decreases the visibility gradually from $V = 0.93$ at 1 keV ($\sigma_E/\rho E_r = 0.0008$) to $V = 0.78$ at 150 keV ($\sigma_E/\rho E_r = 0.125$).

High Brightness SASE
HB-SASE

Mode Locked Optical Klystron undulator/chicane structure, but with different chicane delays*

Each chicane now introduces **different** integer resonant wavelength delay to e^-

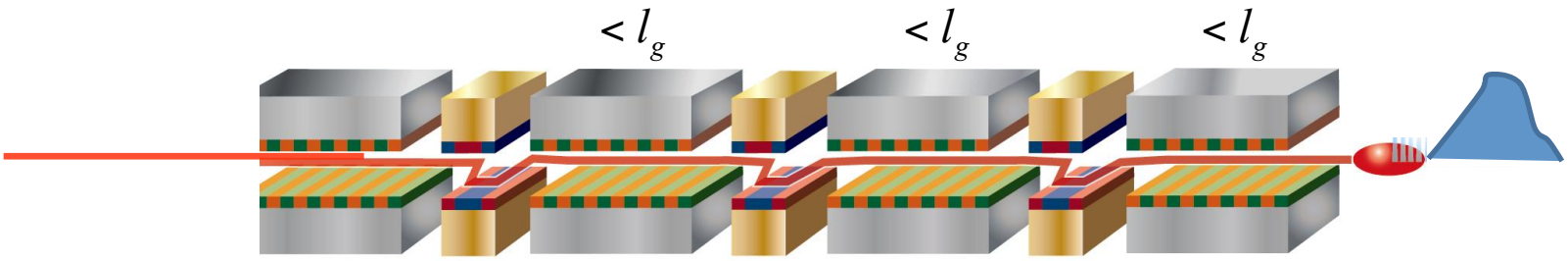

- Only central (resonant) mode remains after many undulator/chicane modules
- For undulator lengths $< l_g$ the coherence length changes from the SASE value of $\sim l_c$ to the total relative electron/radiation slippage length $>> l_c$
- **The localised collective interaction between radiation & electrons has been broken**

*Thompson, Dunning & McNeil, '*Improved temporal coherence in SASE FELs*', **TUPE050**, Proceedings of IPAC'10, Kyoto, Japan

HB-SASE average power

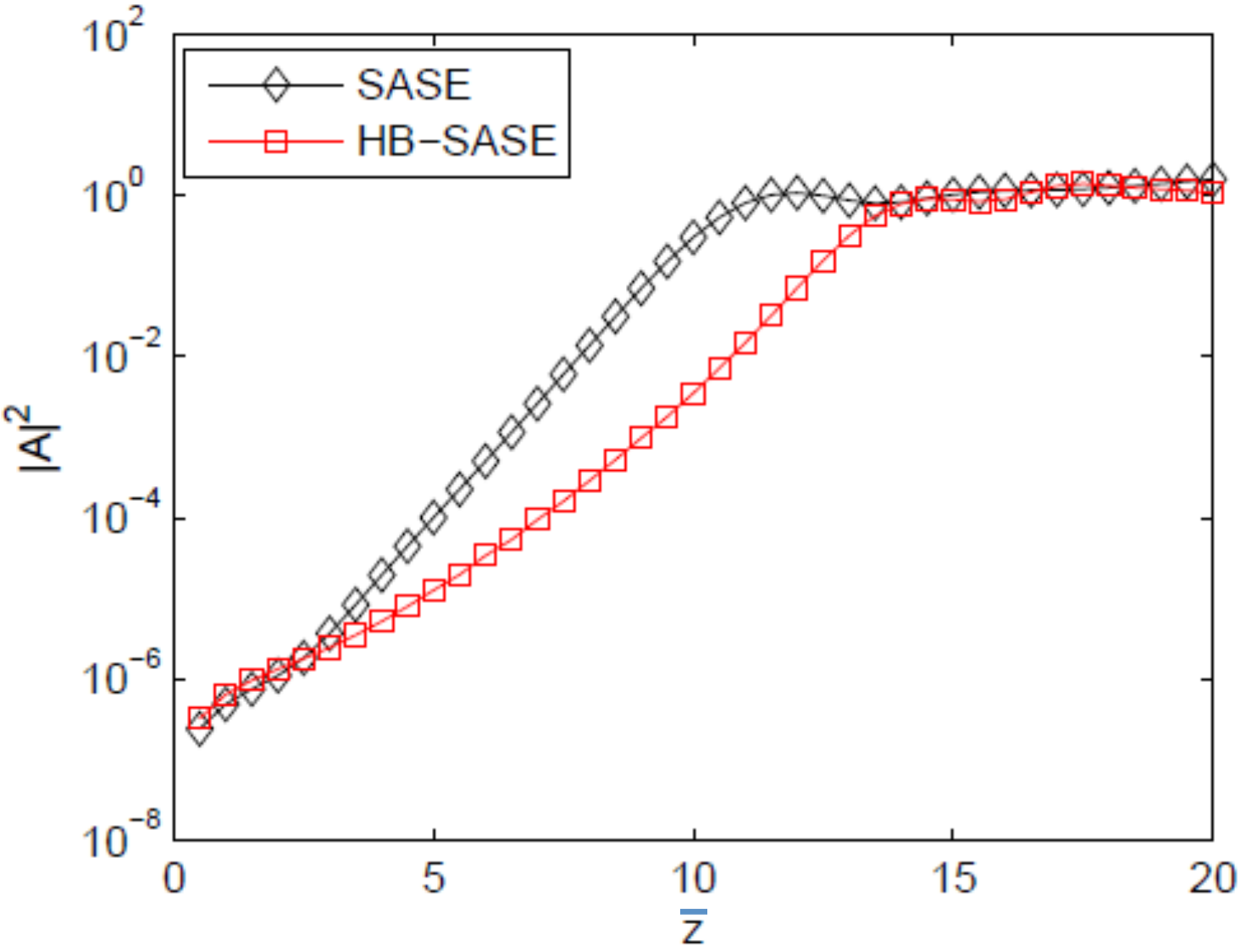

HB-SASE Spectrum for simulation in soft X-ray at 1.24 nm*

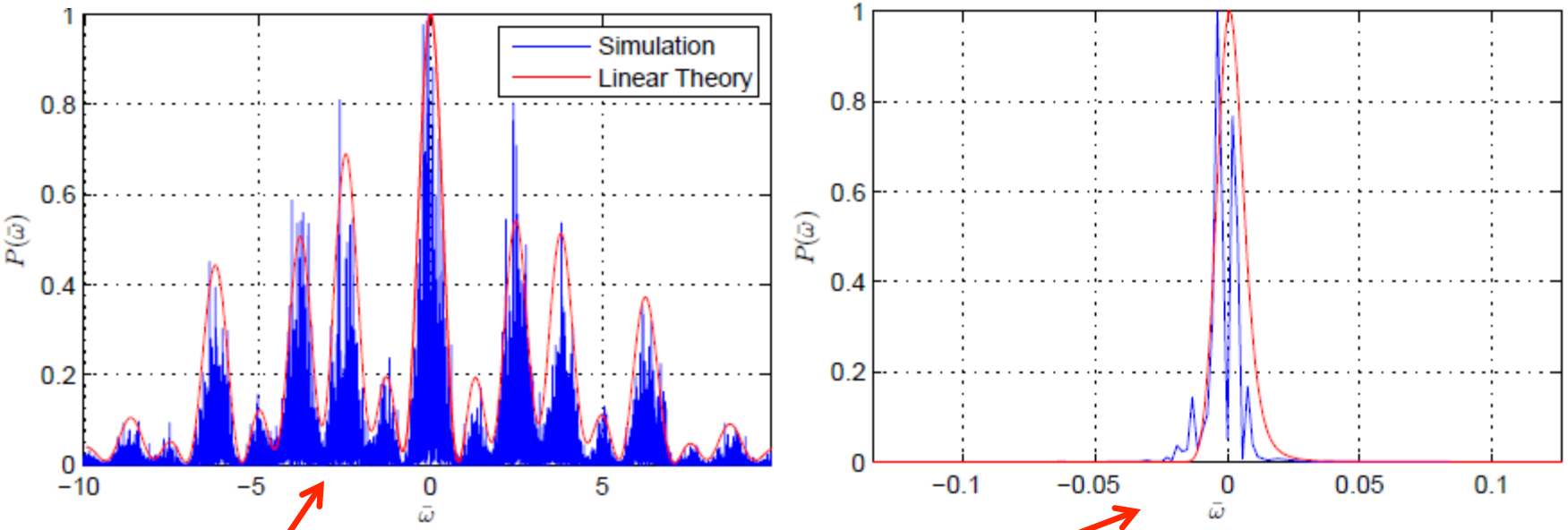

FIG. 3: Comparison of linear theory predictions of FEL spectra with simulation results, for the output after 3 modules (top) and 25 modules (bottom). Note the The x-axis range is adjusted on the bottom plot for clarity.

The system of shifts acts like a 'distributed monochronometer'.

*McNeil & Thompson, 'High Brightness SASE in the Free Electron Laser', in preparation.

SASE & HB-SASE comparison*

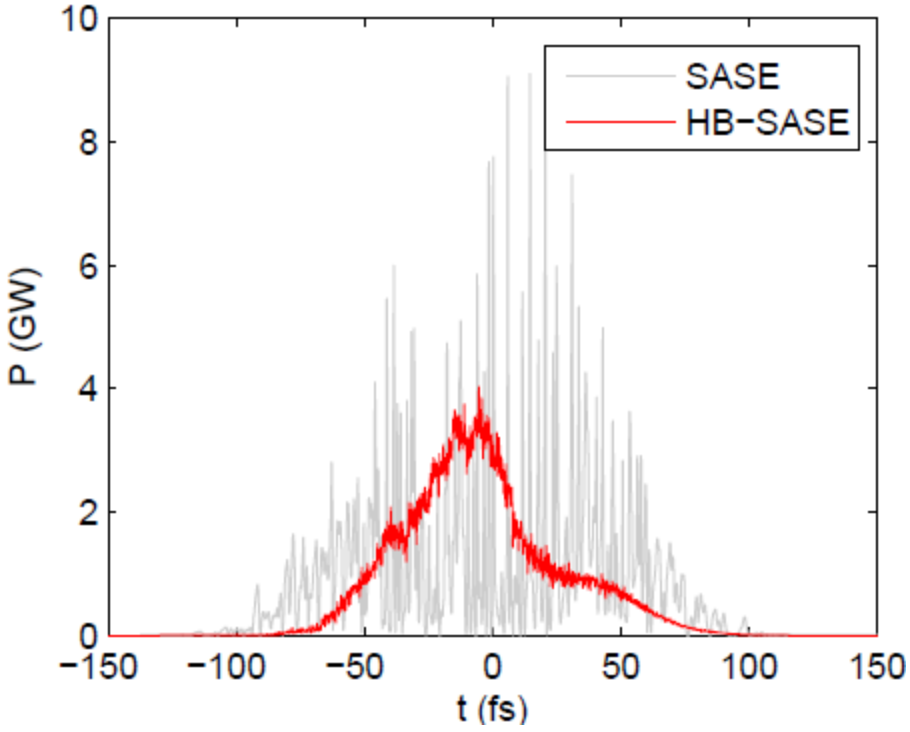

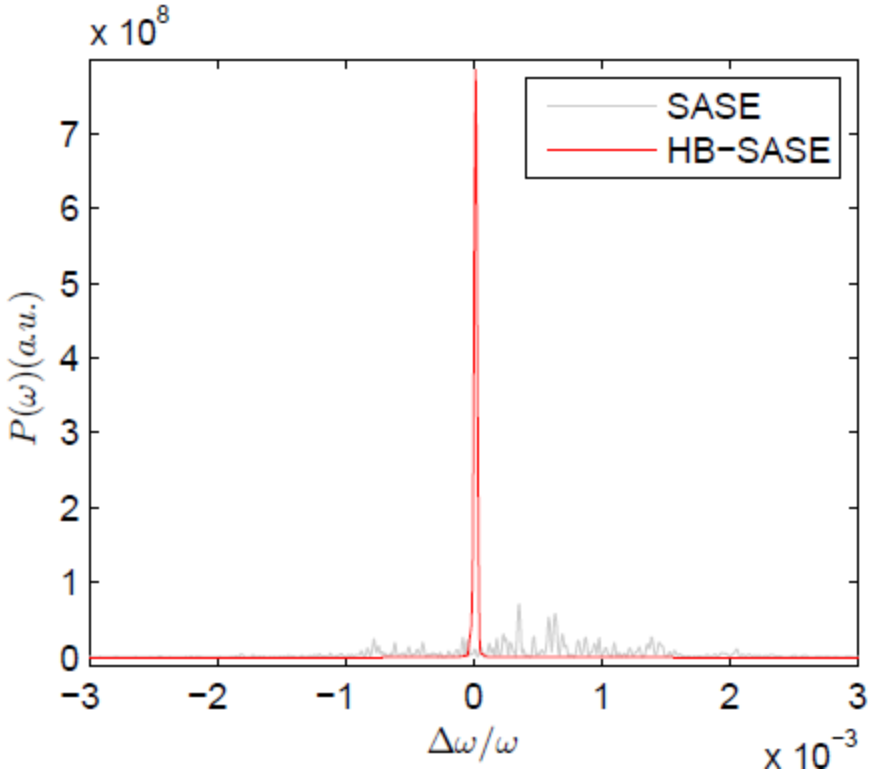

*McNeil & Thompson, 'High Brightness SASE in the Free Electron Laser', in preparation.

Puffin: A three dimensional, unaveraged free electron laser simulation code

(Parallel Unaveraged Fel INtegrator)

PHYSICS OF PLASMAS **19**, 093119 (2012)

Puffin: A three dimensional, unaveraged free electron laser simulation code

L. T. Campbell[1,2,a)] and B. W. J. McNeil[1,b)]
[1]*University of Strathclyde (SUPA), Glasgow G4 0NG, United Kingdom*
[2]*ASTeC, STFC Daresbury Laboratory and Cockcroft Institute, Warrington WA4 4AD, United Kingdom*

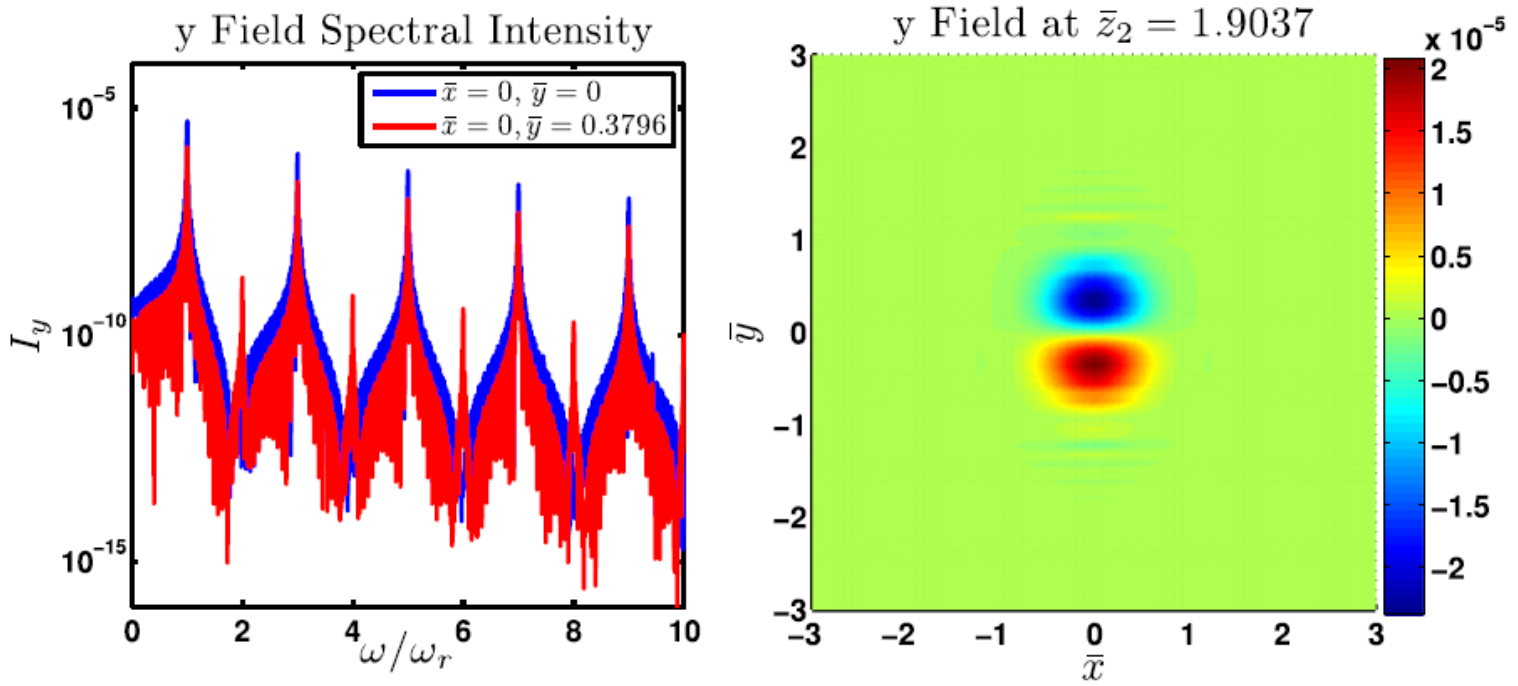

FIG. 4. Left: Spectrum of the y-polarised field. The blue line shows the field at $\bar{x}, \bar{y} = 0$, and the red line is the field at point $\bar{x} = 0, \bar{y} = 0.3796$. Note the even harmonics are only present off-axis. Right: The phase-front of the y-polarised field of the second harmonic at a transverse slice in $\bar{z}_2$ exhibits the expected transverse modal structure.

Non-localised electron evolution & very short pulses*

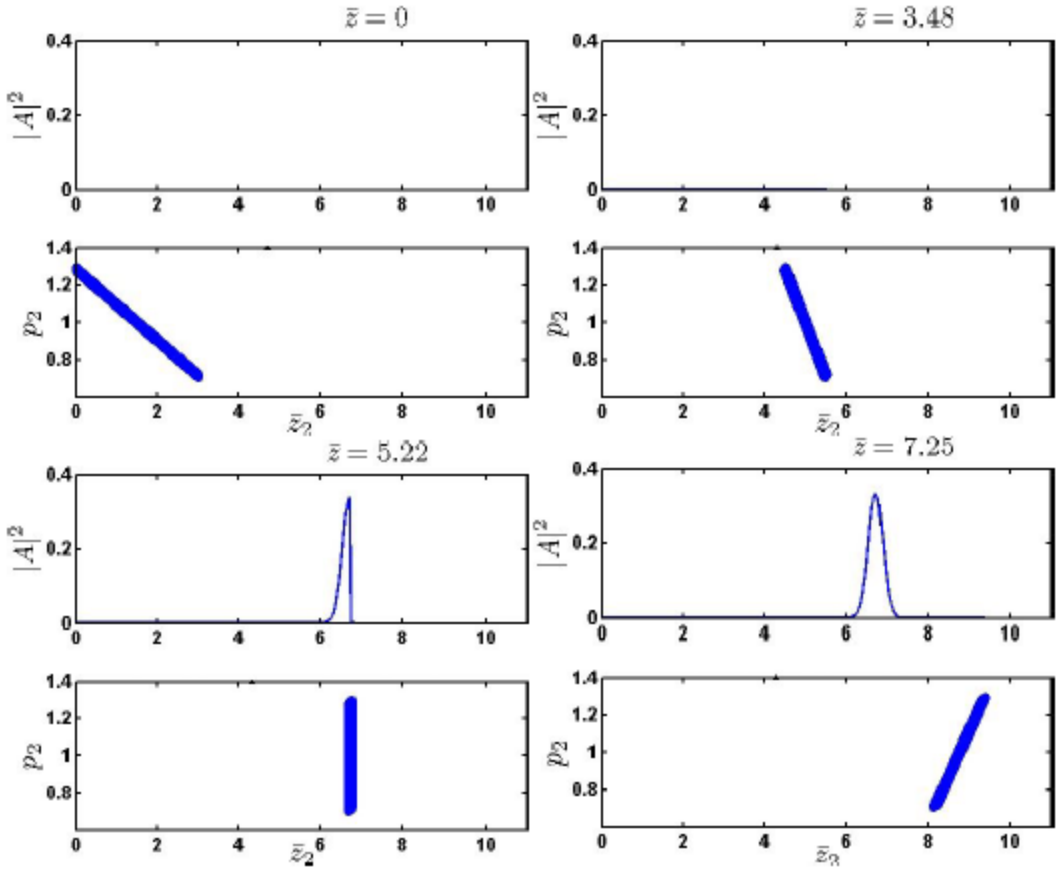

Figure 2: These 8 plots show the intensity and electron beam phase space at 4 different propagation distances. The initial chirp in the plot at $\bar{z} = 0$ in the top left causes the electron pulse to compress and then decompress. When it is bunched to a length in $\bar{z}_2$ of $\lesssim 4\pi\rho$ (that is to say, less than a resonant radiation wavelength) it generates a single coherent spike in intensity.

*Campbell & McNeil, *'A simple model for the generation of ultra-short radiation pulses', Proc. FEL 2012, Nara, Japan.*

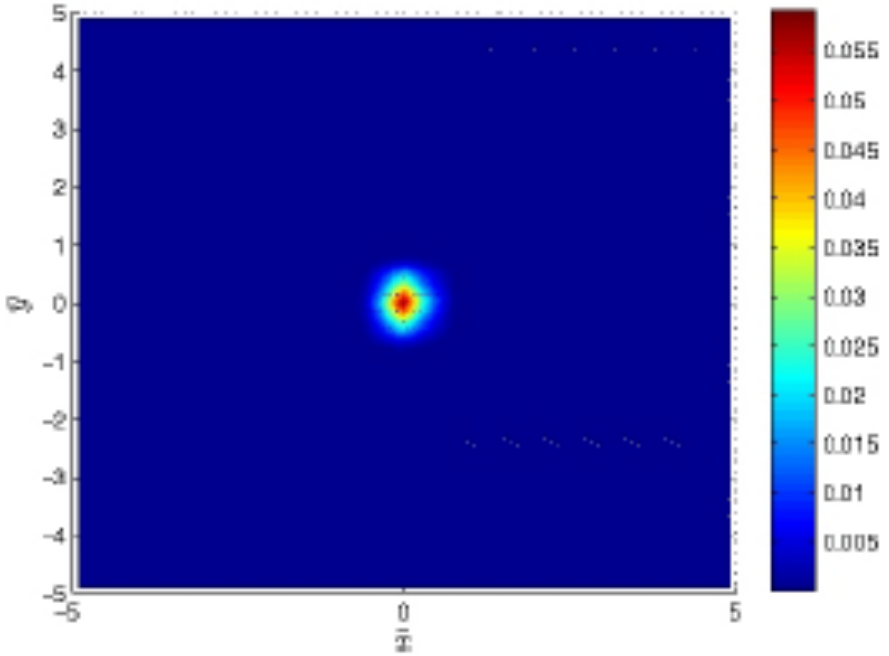

Figure 4: The transverse intensity profile near the peak at $\bar{z} = 7.6676$ and $\bar{z}_2 = 7.0456$ as shown in Fig. 5.

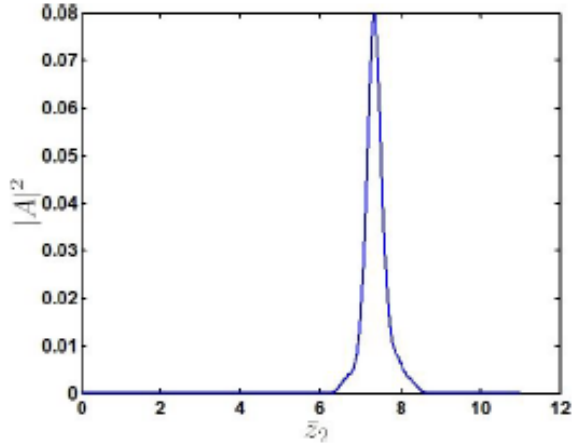

Figure 5: The scaled power $|A|^2$ is calculated by integrating the scaled intensity of Fig. 4 over the transverse area and is plotted as a function of $\bar{z}_2$ for $\bar{z} = 7.6676$.

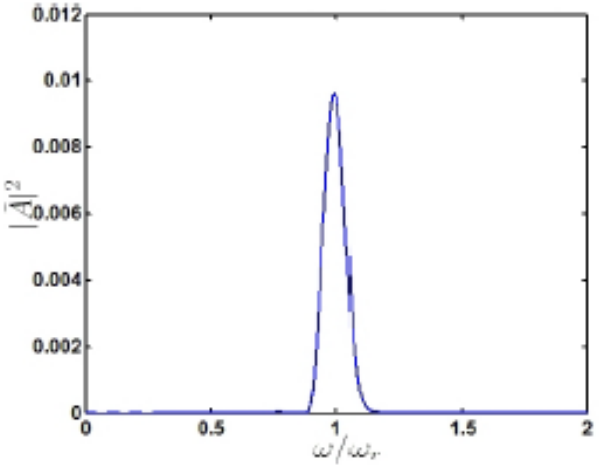

Figure 6: The spectral intensity calculated on-axis along the $\bar{z}_2$ axis at $\bar{z} = 7.6676$.

CLARA – a new UK test facility?*

[**C**ompact **L**inear **A**ccelerator for **R**esearch and **A**pplications]

* Clarke *et al*., **TUPPP066**, Proceedings of IPAC2012, New Orleans, Louisiana, USA
Slides courtesy of Jim Clarke, ASTeC.

To develop a normal conducting test accelerator able to generate longitudinally and transversely bright electron bunches and to use these bunches in the experimental production of **stable**, **synchronised**, **ultra short** photon pulses of coherent light from a single pass FEL with techniques directly applicable to the future generation of light source facilities.

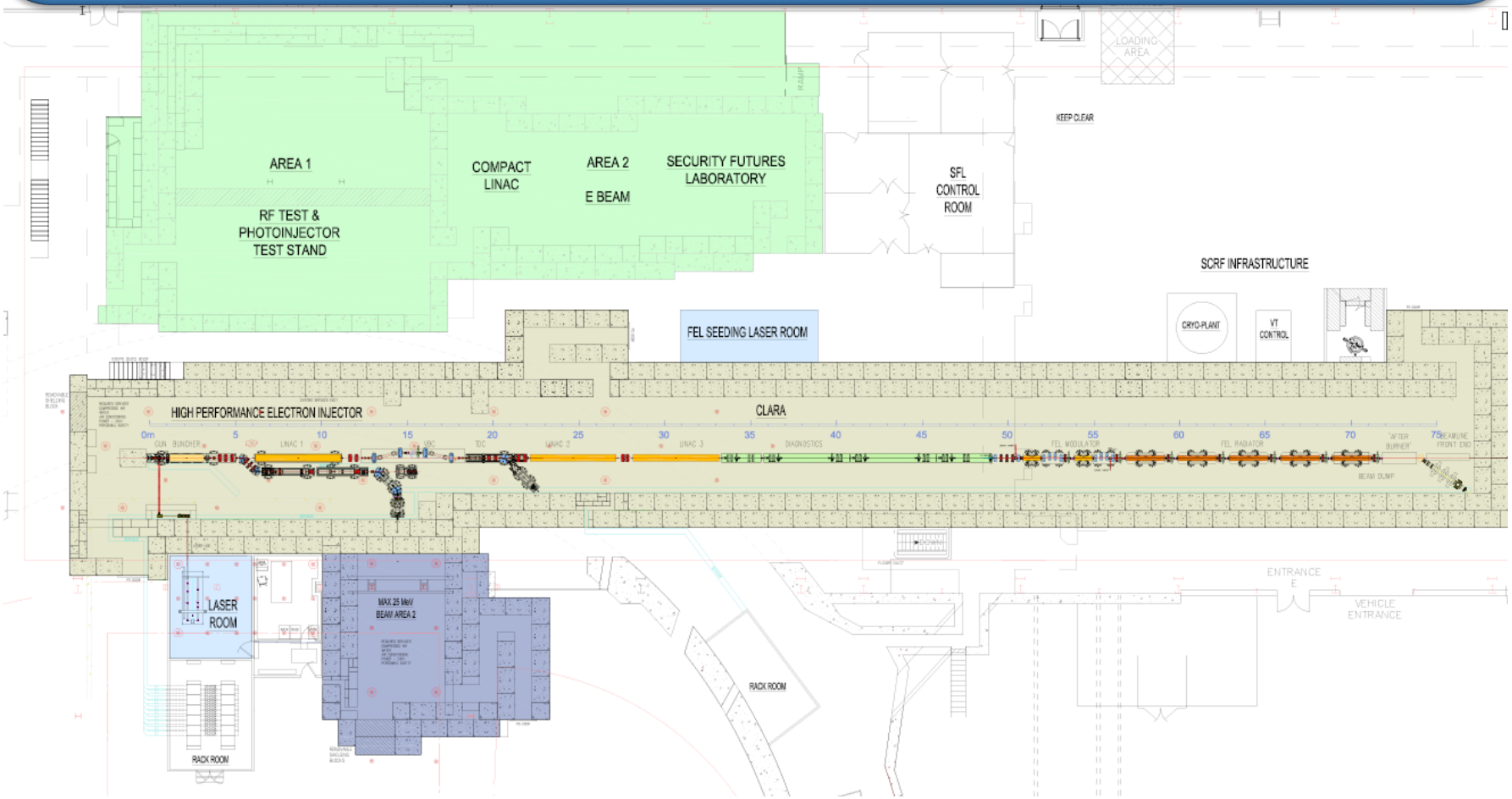

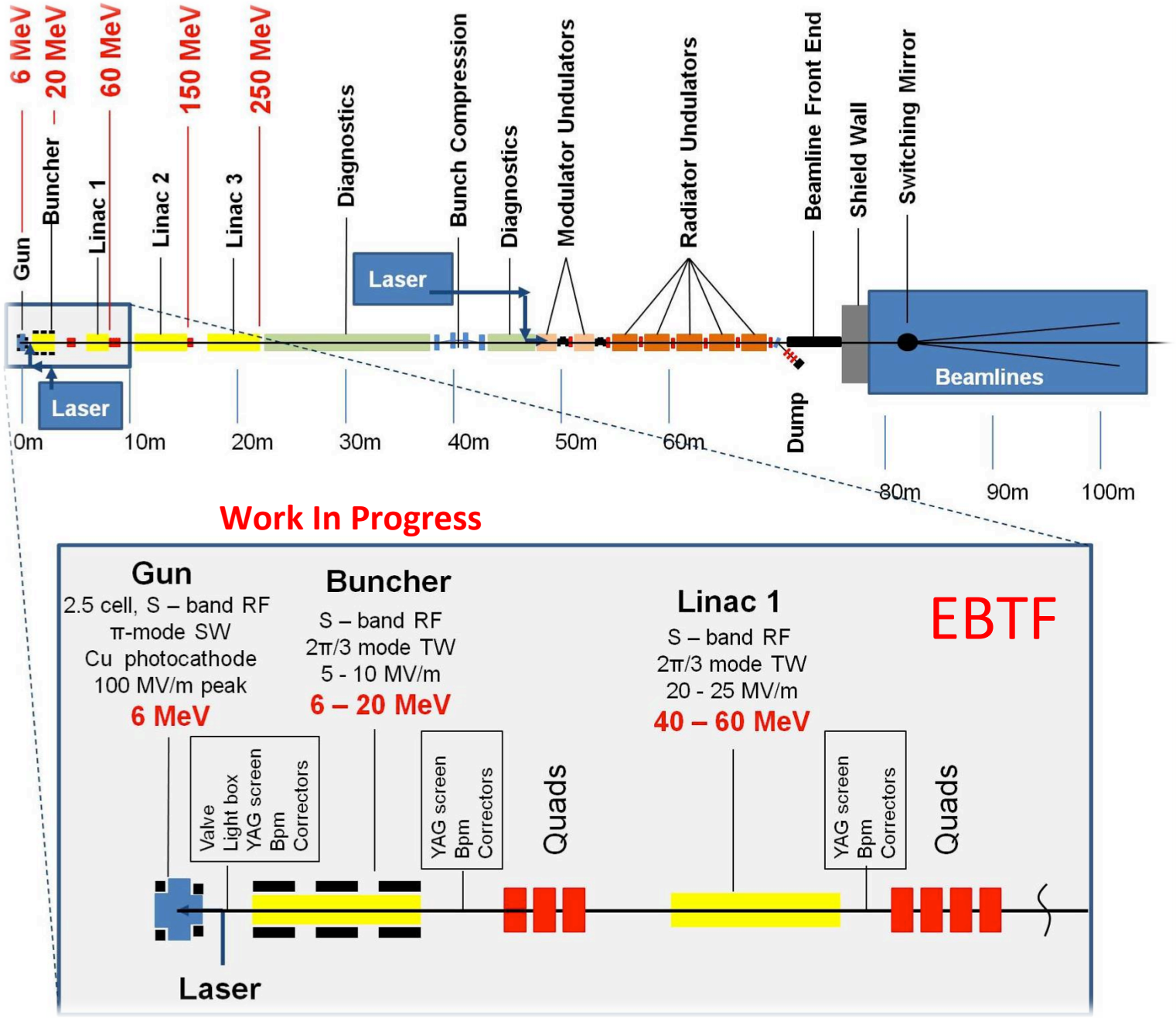
6 MeV
20 MeV
60 MeV
150 MeV
250 MeV
Gun
Buncher
Linac 1
Linac 2
Linac 3
Diagnostics
Bunch Compression
Diagnostics
Modulator Undulators
Radiator Undulators
Beamline Front End
Shield Wall
Switching Mirror
Laser
Laser
Beamlines
Dump
0m
10m
20m
30m
40m
50m
60m
80m
90m
100m
Work In Progress
Gun
2.5 cell, S – band RF
π-mode SW
Cu photocathode
100 MV/m peak
6 MeV
Buncher
S – band RF
2π/3 mode TW
5 - 10 MV/m
6 – 20 MeV
Linac 1
S – band RF
2π/3 mode TW
20 - 25 MV/m
40 – 60 MeV
EBTF
Valve
Light box
YAG screen
Bpm
Correctors
YAG screen
Bpm
Correctors
Quads
YAG screen
Bpm
Correctors
Quads
Laser

CLARA Timeline

- Outline Design of CLARA – Dec 2012
- Design Report and Costing – March 2013

- CLARA construction – 2013 to 2015
- CLARA first commissioning – 2016

} Funding required!

Thank You!

Feasibility III - Stability

2.1 Energy Spread

High-gain optical klystron theory [1] gives a criterion for operation which relates the electron beam energy spread to the dispersive strength of the chicane:

$$\bar{\sigma}_\gamma \equiv \frac{\sigma_\gamma}{\rho\gamma} \lesssim \frac{1}{D},$$

where $D = 2\pi\rho R_{56}/\lambda_r$ and $R_{56} \simeq 10\delta/3$ is the momentum compaction factor, with δ the chicane delay, giving

$$\sigma_\gamma < \frac{3\lambda_r}{}$$

Using

	XUV	X-ray
$\sigma_\gamma/\gamma < 1/20N_c$	1×10^{-3}	2×10^{-4}
$\Delta B/B < 1/(2N_c\sqrt{N})$	2×10^{-3}	4×10^{-4}

Table 2: Required tolerances for SASE mode-locking, for the XUV and X-ray cases.

2.3 I

The effe
the synt
resonan

he toler-

$$\lambda = \frac{\lambda_w}{2\gamma^2}(1 + a_w^2) \qquad (4)$$

where $\gamma = E/E_0$ for a relativistic beam, the delay in units of resonant wavelengths is then given by

$$\frac{\delta}{\lambda} = \frac{2L^3B^2c^2}{\lambda_w E_0^2(1 + a_w^2)}$$

which is independent of the beam energy so that as the beam energy fluctuates the chicanes always delay by exactly the same number of resonant wavelengths. This means that although the resonant wavelength may vary the development of the axial mode structure is unaffected.

2.2 Magnet Stability

The delay in a 4-dipole chicane with equal magnet and drift lengths, L, may be written as

$$\delta = L\phi^2 \qquad (3)$$

where ϕ is the deflection angle which is assumed to be small. For a relativistic beam the deflection angle in a single dipole of length L and field strength B is

$$\phi = \frac{LBc}{E}$$

where E is the beam energy in units of eV. Therefore from (3)

om walk

so that the tolerance over N modules will be reduced by $1/\sqrt{N}$ to give

$$\frac{\mathrm{d}B}{B} < \frac{1}{2N_c\sqrt{N}}.$$